Research on Stable, High-Efficiency, Amorphous Silicon Multijunction Modules

Annual Subcontract Report
1 May 1991 — 30 April 1992

A. Catalano, M. Bennett, L. Chen,
R. D'Aiello, B. Fieselmann, Y. Li,
J. Newton, R. Podlesny, L. Yang
Solarex Thin Film Division
Newton, Pennsylvania

NREL technical monitor: W. Luft

◆NREL

MASTER

On September 16, 1991 the Solar Energy Institute was designated a national laboratory, and its name was changed to the National Renewable Energy Laboratory.

NOTICE

DISCLAIMER

Portions of this document may be illegible electronic image products. Images are produced from the best available original document.

EXECUTIVE SUMMARY

Goal: The primary goal of the Phase II effort is to demonstrate a multijunction module with a "stabilized" efficiency (600 hrs., 50°C, AM1.5) of 10.5%.

Approach: Triple-junction devices and modules employing a-Si:H alloys with carbon and germanium will be developed in order to meet program goals. ZnO will be used to provide a high optical transmission front contact.

Introduction

Proof of concept has been obtained for several important advances we felt were essential for obtaining high (12.5%) "stabilized" efficiency. These are 1) stable, high quality a-SiC:H devices and 2) high transmission, textured zinc oxide (ZnO). Although these developments have not been scaled up and included in modules, we have demonstrated initial triple-junction module efficiencies as high as 10.85%. NREL measured 9.62% and 9.00% indoors and outdoors, respectively. The modules are expected to lose no more than 20% of their initial performance.

Task I: Semiconductor Materials and Device Research

Triple-junction devices with the structure a-SiC:H/a-Si:H/a-SiGe:H have yielded an open circuit of 2.55V. The high V_{oc} results from the incorporation of a-SiC:H as the top junction in the triple-bandgap, triple-junction structure. Incorporating a-SiC:H layers into the triple-junction device is a consequence of the favorable results of efforts to develop device-quality a-SiC:H. These efforts have proven successful owing to the use of novel feedstocks such as di- and tri-silylmethane (DSM, TSM) and the use of high hydrogen dilution of the conventional feedstock, methane. Of particular importance is the fact that recently developed a-SiC:H devices degrade at a rate comparable, though slightly higher than the best conventional a-Si:H devices. In the range of thickness necessary for triple-junction devices (i.e. $\leq$ 2000Å) the rate of degradation is acceptable. The use of DSM and TSM as the source of carbon for a-SiC:H devices is based on the paradigm that feedstock gases which incorporate the preferred Si-C bonds will give rise to such desirable bonding in the semiconductor film leading to superior transport properties, and devices. This hypothesis is supported by experimental results that confirm that the usual mea-

sures of film quality, namely Urbach Energy, minority carrier diffusion length, photoconductivity and midgap absorption are all superior to films prepared from methane using a conventional process. **Devices based on these novel feedstocks have achieved a V_{oc} approaching 1V.**

Hydrogen dilution of methane at a ratio of 20:1 (H_2:CH_4+SiH_4) has also yielded a substantial increase in film and transport properties. Furthermore, because our supply of methane is unlimited, the opportunities are much greater to optimize the process. Films prepared under optimum conditions exhibit properties comparable to those of films prepared from DSM and TSM. a-SiC:H devices with an V_{oc} as high as 0.981 and good fill factor (> 63%) have been obtained.

The model based on a stretched exponential time dependence has been extended and refined to describe the time dependent behavior under a variety of conditions. An essential feature of the model is the attainment of a steady state performance determined by the balance between defect creation via light exposure or electrical bias and thermal annealing. The model also includes such practical considerations important to device design as i-layer thickness. The experimental measurement of the variation in degradation with electrical bias has been compared using an established device model. Best agreement with theory occurs for the case in which the rate of degradation is determined by recombination between a free hole and trapped electron.

Task II: Non-Semiconductor Materials Research

Development of a continuous atmospheric pressure chemical vapor deposition (APCVD) process for coating glass with ZnO has been undertaken and successfully passed the proof-of-concept stage. The APCVD process employs diethylzinc (DEZ), water and ethanol doped with fluorine from either HF or hexafluoropropylene to produce films ranging from specular to very high (~ 70%) haze. The basic process (gas flows, exhaust rate, temperature, etc.), have been defined. Films grown by APCVD appear to consist of tightly packed "nodules" as compared to the well-faceted crystal faces evidenced by films prepared by low pressure chemical vapor deposition (LPCVD).

Careful optical transmission measurements were performed by immersion of films in an index matching fluid. Such measurements confirmed peak transmissions of over 90% for APCVD ZnO films compared to approximately 83% for a SnO_2 control. The superior transmission of the ZnO films is confirmed by device measurements that have shown **peak quantum efficiencies as high as 93.6% for devices on ZnO** compared to 85% for devices on a SnO_2 control.

Unfortunately, devices prepared on ZnO usually exhibit a high series resistance and/or low V_{oc}. The difficulty is apparently due to a barrier at the p/ZnO interface. Increasing the *p*-layer conductivity appears to reduce the problem associated with the contact. Further work is needed to fully understand and correct the ZnO/p interfacial problems.

Task III: Module Research

Although the development of Task I and Task II of a-SiC:H and ZnO auger well for the development of high efficiency modules that will meet the program goals, these processes were not sufficiently mature to include in modules during Phase II. Nonetheless, using SnO_2 coated glass and a dual bandgap, triple-junction device structure of the type a-Si:H/a-Si:H/a-SiGe:H, we developed modules that had a measured initial aperture area conversion efficiency as high as 10.85%. This device design has been shown to degrade no more than 20% in tests on small area devices, so that we expect the stabilized performance to be in the neighborhood of 8.7%. By incorporating the developments under Tasks I and II (a-SiC:H and ZnO), we expect an increase in the initial module efficiency to the range of 12.5% with little or no increase in degradation.

Calculations based on our model of the degradation process have been made which indicate measurable discrepancies will occur as a consequence of exposure to various light sources. Light sources such as Na-vapor and Vortek lamps have their output concentrated at various parts of the spectrum leading to over/under degradation of individual junctions of the cells in multibandgap, multijunction cells. The extent of the deviation from the ideal case of time AM1.5 illumination depends on the structure (tandem, triple-junction) and bandgap of the individual junctions.

TABLE OF CONTENTS

LIST OF FIGURES

LIST OF FIGURES

LIST OF FIGURES

LIST OF TABLES

1.0 INTRODUCTION

During Phase II of the program, we have made excellent progress toward realizing the goals stated in our original proposal which we expect will lead to stabilized module efficiencies of 12.5%. We believe the highest "stabilized" efficiencies can only be obtained using a triple-junction, triple-bandgap structure. Extensive modeling has demonstrated that such a design is capable of 24% using a 2.0 eV top junction and 1.45 eV bottom junction. Therefore, we have sought to develop stable, high performance a-SiC:H devices for the top junction. The lower bandgap junction (a-SiGe:H) was optimized for initial performance and stability earlier but may require further refinement. The other key element of our strategy has been to develop a very high transmission, textured transparent front contact. ZnO has been selected for this purpose and we have been actively developing an APCVD process.

We are pleased to report that results in these two areas (a-SiC:H and ZnO) have been highly favorable and we now have passed the proof-of-concept stage for both elements of our strategy. Because these processes had not yet been scaled up, we have not included them in modules. Nonetheless, many modules over 10% aperture area conversion efficiency have been prepared using a dual bandgap triple-junction structure. The highest conversion efficiency measured was 10.85% using a design that we anticipate will permit no more than a 20% degradation.

1

2.0 TASK I: SEMICONDUCTOR MATERIALS RESEARCH

2.1 a-SiC:H Cells with High V_{oc} Values

In order to enhance the performance of a-Si:H based multijunction solar cells, higher V_{oc} values are needed without substantial loss in fill factor (FF). Higher V_{oc} can result from either improved doped layers (higher built-in potential) and/or wide-gap i-layers. The latter approach means using high bandgap a-Si:H alloys, such as a-SiC:H, as the absorber in the first junction of multijunction cells. In this report period we have concentrated on the development of high V_{oc} cells. Simple p-i-n single junction solar cells have been prepared using undoped wide-gap a-SiC:H i-layers, which were deposited both from methane+silane mixtures with heavy hydrogen dilution (the CH_4+H_2 recipe) and from novel carbon feedstocks trisilylmethane (TSM) and disilylmethane (DSM). These cells exhibit high FF and V_{oc} values. Preliminary cell stability tests under intense illumination have been conducted with encouraging results. Approximately a 10% increase in V_{oc} has been demonstrated in triple-junction cells by using wide-gap a-SiC:H i-layer and a-Si:H i-layer in the first and second junctions, respectively.

Our earlier study on a-SiC:H alloy films has established that the rather poor properties, such as small diffusion length of photo-generated holes, of CH_4 based undoped a-SiC:H alloys produced by glow-discharge can be significantly improved by either heavy hydrogen dilution (1) (the $CH_4 + H_2$ recipe) or by using novel carbon feedstocks such as TSM $[SiH_3]_3CH$ with built-in Si-C bonds (2). However, as described in our last report (3), *good film (i-layer) properties often do not simply translate into high solar cell efficiency*, as illustrated by the rather poor performance (notably low V_{oc}) of some earlier a-SiC:H cells based on CH_4+H_2 or TSM (4). By modifying the deposition process required for making good films, we have succeeded in adapting the film-growth recipes to solar cell preparation. The p-i-n solar cells, made by rf glow-discharge in capacitively coupled diode reactors, were of the glass/SnO/p^+-SiC/i-SiC/n-Si/ZnO/Ag structure with conventional doped layers.

Table 2-1 lists the V_{oc}, short circuit current (J_{sc}), FF, and efficiency of selected a-SiC:H cells. The i-layer thickness (in Å) is close to what would be needed for the top absorber in triple-junction cells (5). Also listed is the quantum efficiency (QE) measured at the wavelength of 400 nm. DSM in **Table 2-1** refers to the novel carbon source DSM (4). As we reported the last time, it is not clear why the DSM based cells perform very well (initially) despite the mediocre film properties which are comparable to those of CH_4 based films without H-dilution. The high V_{oc} and high FF shown in **Table 2-1** are not obtainable using CH_4 based a-SiC:H alloys without H-dilution. As a comparison, single junction cells using a-Si:H i-layers with CH_4 (no H-dilution)

Table 2-1. Parameters of Selected *p-i-n* a-SiC:H Solar Cells.

Cell I.D.	*i*-layer Carbon Feedstock	*i*-layer Thick-ness	QE @ 400 nm	V_{oc} (V)	J_{sc} mA/cm^2	FF	Effi-ciency
S202130	None (a-Si)	3,500	0.66	0.858	15.2	69.7	9.1
C2077-7	CH_4+H_2	2,000	0.56	0.908	9.65	70.3	6.2
C2077-3	CH_4+H_2	2,000	0.55	0.925	9.81	70.3	6.4
C2077-1	CH_4+H_2	2,000	0.53	0.946	7.97	67.4	5.1
C2076-4	CH_4+H_2	2,000	0.65	0.955	9.91	68.2	6.5
C2076-3	CH_4+H_2	2,000	0.61	0.967	9.11	66.9	5.9
C2063-5	CH_4+H_2	2,000	0.66	0.981	8.04	63.6	5.0
S20226M	TSM	1,000	0.74	0.911	9.82	68.1	6.1
S20227O	TSM	750	0.75	0.931	7.89	75.1	5.5
S20228Q	TSM	700	0.73	0.941	7.29	72.1	5.0
S20225J	TSM	800	0.76	0.951	7.99	67.4	5.1
S20401K	TSM	850	0.55	0.978	5.81	65.2	3.6
S20220G	TSM	1,000	0.73	0.991	7.61	61.9	4.7
S20305W	DSM	?	0.73	0.945	7.91	72.3	5.4
S20306A	DSM	?	0.75	0.942	8.11	72.2	5.7
S20309C	DSM	?	0.74	0.961	8.29	64.8	5.2

usually limits V_{oc} to about 880-900 mV. The fill factors and stability of devices is usually poor, too. However, for cells with a V_{oc} in the mid-900 mV range and a FF of near 0.7 can be obtained using both the novel polysilylmethane (TSM or DSM) *and* the more practical CH_4+H_2 recipes. Data to date indicate that high quality a-SiC:H cells can be made from the conventional carbon source methane under carefully chosen conditions without using novel carbon feedstocks (TSM and DSM), although the latter seem to make it easier in finding good deposition recipes presumably due to absence of high density of CH_4 radicals in the plasma. It is remarkable that a V_{oc} approaching 1V could be attained, with only mild loss in FF (> 0.6) by using conventional

doped layers, via an improvement in the i-layer quality alone. Further increase in V_{oc} may result from optimizing doped layers (p and/or n) to enhance the built-in electrical potential or from the use of buffer layers.

The short wavelength QE or "blue response", measured at 400 nm, has been found to be discernibly lower for the CH_4+H_2 based a-SiC:H cells compared to the TSM based cells, although both types of cells exhibit high V_{oc} and high FF. The QE curves for two TSM and CH_4+H_2 cells with V_{oc} near 0.96V, along with that of an a-Si:H cell without any p-i buffer, are displayed in **Figure 2-1**. The relative QE values show superior blue response, on average, for the TSM based cells compared to a-Si:H control cells and CH_4+H_2 based a-SiC:H cells. This is unexpected from the study of *film* properties which are quite comparable for the CH_4+H_2 based and the TSM based films (with bandgap near 1.9 eV). The heavy hydrogen dilution in the deposition of CH_4+H_2 based i-layers may lead to excessive etching of the p-layers and lower the blue QE.
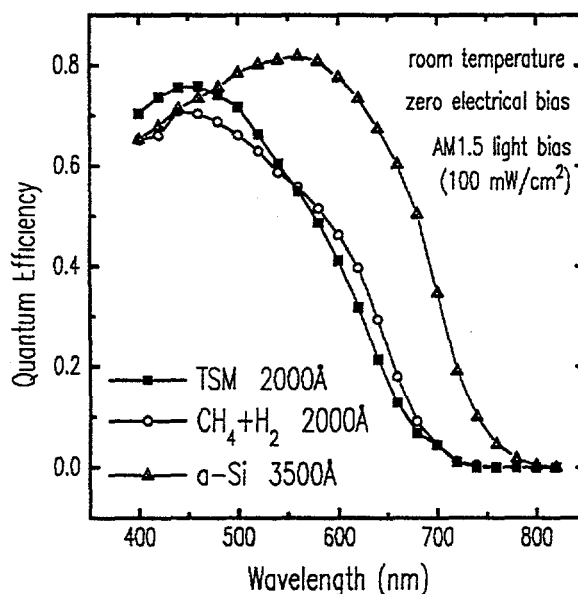
Figure 2-1. Representative QE spectra of TSM and CH_4+H_2 based a-SiC:H cells compared to an a-Si:H control cell.

Wide-gap a-SiC:H alloys, based on either CH_4+H_2 or TSM (and DSM) have also been successfully incorporated in a-Si:H (i) single junction solar cells as the buffer (grading) layers between the p and i to boost the V_{oc}. The improved buffers have led to relatively high V_{oc} (for a-Si:H i-layer devices) without degrading the FF, as compared to the CH_4 based buffers without hydrogen

4

dilution. High quality buffers are expected to be useful in, e.g., the middle junctions of triple-junction cells. Finally, high V_{oc} values of 2.55V have been demonstrated in triple-junction solar cells (a-SiC/a-Si/a-SiGe) using $CH_4 + H_2$ based a-SiC:H as the top junction i-layer. The cell structure is yet to be optimized (e.g., better current matching) for high conversion efficiency.

We showed in the last report that the stability against light-soaking of a-SiC:H cells can vary with deposition conditions for a *given bandgap*. The poor stability of CH_4 based glow-discharge a-SiC:H alloys can be improved by depositing from hydrogen diluted methane (20:1, H_2: $CH_4 + H_2$) which reduces the density of CH_3 bonds in the alloy which we presume is the cause of the faster degradation of a-SiC:H compared to a-Si:H. **Figure 2-2** shows the degradation history of a $CH_4 + H_2$ based wide-gap solar cell ($V_{oc} > 0.96V$), along with that of an a-Si:H cell made under the same conditions without CH_4, under strong illumination (Xe lamp filtered by H_2O) whose intensity was about 50 times that of the AM1.5 level. The stability of the a-SiC:H cell is only mildly inferior at short times to that of the a-Si:H cell (and is much better than the CH_4 based cells with comparable initial V_{oc}). The true stabilized performance cannot be determined from this data. Although the a-SiC:H looks somewhat worse, shunting in the cells was noted at long times and may confuse the result. Of course, this kind of comparison is not straightforward because the a-SiC:H cell absorbs less light due to its higher optical bandgap than a-Si:H. However, the J_{sc} of the device is comparable to that required in the proposed triple-junction device.
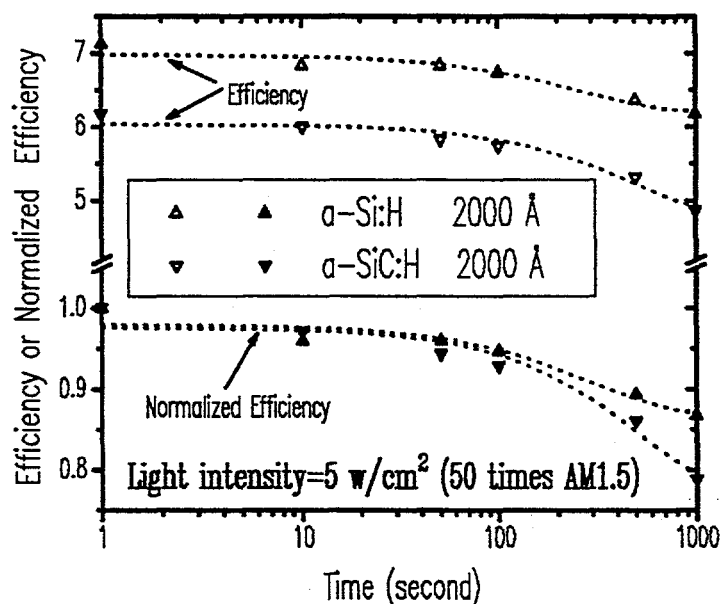
Figure 2-2. Time evolution of efficiency and normalized efficiency of a $CH_4 + H_2$ based a-SiC:H cell (initial V_{oc} = 0.967V) and an a-Si:H cell under intense illumination (temperature near 50°C).

5

Figure 2-3 displays the variation with V_{oc} of the fill factor of CH_4+H_2 based a-SiC:H solar cells before and after 1000 seconds of intense optical illumination (50 times AM1.5 intensity). The FF decreases with increasing V_{oc} in accordance with increasing defects in the i-layer (i=2000Å). The FF after the accelerated degradation is much higher than what can be expected from CH_4 based cells. For unalloyed a-Si:H, the above light-soaking would be equivalent to over 300 hours of AM1.5 (100 mW/cm^2) illumination due to the supra-linear dependence of defect creation rate on light intensity (6), assuming the scaling law relating light intensity and exposure time holds for wide-gap a-SiC:H solar cells. Direct degradation measurements under AM1.5 conditions (100 mW/cm^2) will be needed to establish the stability of these a-SiC:H cells. Available data suggest that acceptable stability for a-SiC:H solar cells with high V_{oc} (high bandgap i-layers) should be obtainable by carefully optimizing the deposition process.
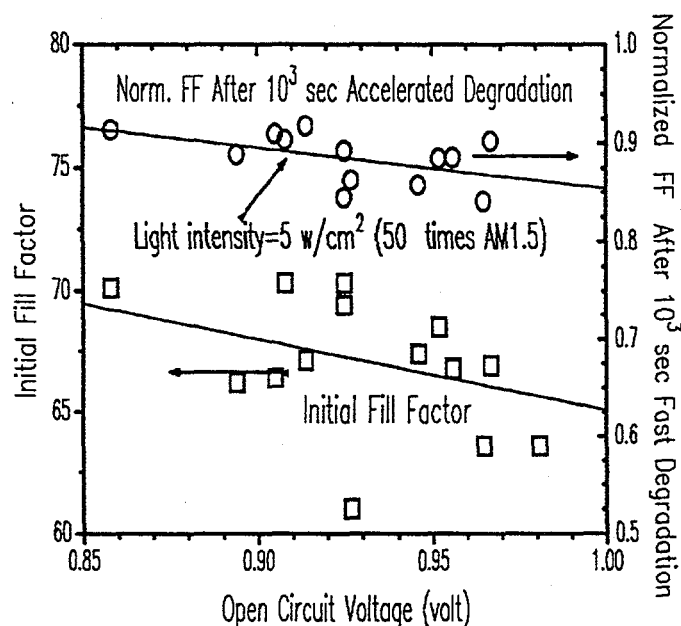
Figure 2-3. The initial and final fill factor (after 10^3 sec. of intense illumination) of CH_4+H_2 based a-SiC:H solar cells as a function of the initial V_{oc}.

In summary, significant progress has been made toward preparing high V_{oc} single junction solar cells with high fill factor using wide-gap a-SiC:H alloys as the i-layers. The high quality i-layers were prepared either by using heavy H_2 dilution of the CH_4+SiH_4 mixtures or by using novel carbon feedstocks TSM and DSM. Preliminary data from light-induced degradation tests under intense illumination indicate that the instability of the a-SiC:H solar cells of high V_{oc} can be substantially reduced by employing the hydrogen dilution method. A better understanding of the long term performance of these devices awaits further tests.

2.2   Research on Novel *P*-layers

Other than using a wide bandgap semiconductor *i*-layer as we discussed in the previous section, the V_{oc} of the solar cells can be also improved by developing better doped layers. The present a-SiC:H *p*-layer made by glow discharge of SiH_4+CH_4 gas mixture has relatively low conductivity ($\sim 10^{-4}$ $W^{-1} \cdot cm^{-1}$) and high activation energy (~ 0.4 eV) which limits the built-in potential of the solar cell. On the other hand, the performance of solar cells could also be sensitive to such factors as the interface defect density and the junction band alignment which are relatively difficult to examine experimentally. Therefore, the goal of research on alternative *p*-layers is to increase the dark conductivity, decrease the conductivity activation energy, and ultimately to demonstrate an improved cell performance. We have pursued a strategy of developing novel amorphous (a-SiC:H, a-SiO:H) on microcrystalline doped layers for this purpose.

2.2.1   a-SiC:H *p*-layer Made by DSM

It is now become clear that the electronic properties of the intrinsic a-SiC:H alloy can be greatly improved by using DSM or TSM as the C containing feedstock instead of methane. These novel feedstocks help reduce such undesirable microstructures as the methyl groups (CH_3) in the alloy material and thus the density of defect states. In this study, we have explored the use of DSM for depositing a-SiC:H *p*-layers. Although the same deposition conditions which had produced good intrinsic alloy films were adopted for the p-layer deposition, the conductivity and the activation energy of the p-layer were not significantly improved as compared to the methane based films. This observation is believed to result from the fact that the electronic properties of the *p*-layers are predominantly controlled by dopant induced defects and thus are less sensitive to the change in the intrinsic alloy properties. Nevertheless, we have incorporated such *p*-layers made with DSM in solar cells and found that the device V_{oc} values were actually improved by an appreciable amount from those of methane based control cells. The typical device results are summarized in **Table 2-2**. These devices had simple *p-i-n* structures, with no buffer layers at interfaces, in which the *i*-layer thickness was about 2100Å. The V_{oc} values of 0.87 - 0.88V are about 40 mV higher than that of the control cells without interface buffer layers. While some degree of H_2 dilution is used in preparing the DSM based *p*-layers, it was found to be important to avoid H_2 dilution at the SnO_2/p-layer interface or lower blue QE response would result. It is yet to be understood why *p*-layers made with DSM lead to higher V_{oc} values as no obvious improvement was observed in the properties of doped films. *However, it is well known that the quality of p/i interface*, which can be drastically modified by using DSM, *plays an important role in determining the V_{oc} of the device.*

7

Table 2-2. Simple p/i/n Cells with a-SiC:H p-layers Using DSM as a Source of Carbon & With H_2 Dilution (Without any p/i Grading or Buffer).

Cell #	Depos. Time (s)	H_2 Grading @ CTO/p	Q.E. @ 400 nm	V_{oc} (V)	J_{sc} (mA/cm^2)	FF (%)	Eff. (%)
S20320V	100	no	0.432	0.866	11.3	62.1	6.07
S20323Y	110	no	0.381	0.871	11.1	56.4	5.46
S20327E	102	yes	0.570	0.871	12.7	69.4	7.68
S20330G	85	yes, short	0.585	0.859	13.0	69.8	7.81
S20330H	95	yes, short	0.541	0.881	12.9	69.1	7.85
S20331J	95	yes, short	0.575	0.867	12.5	68.1	7.38

2.2.2 a-SiO:H p-layer

Following the report of the Fuji group (7) which found that boron doped a-SiO:H p-layer has led to good quality p-i-n cells, we have explored the optoelectronic properties of both intrinsic and p-type a-SiO:H alloys made with mixtures of SiH_4 + CH_4. Perhaps contrary to expectation, the properties of the undoped a-SiO:H alloys with bandgaps from 1.84 to 2.0 eV are noticeably better than those of CH_4 based a-SiC alloys without H-dilution. **Figure 2-4** shows the comparison of photoconductive $\mu\tau$ product, ambipolar diffusion length, Urbach energy, and subbandgap absorption between a-SiO:H and a-SiC:H as a function of bandgap. The "undoped" a-SiO:H

(a)

8

(b)

(c)
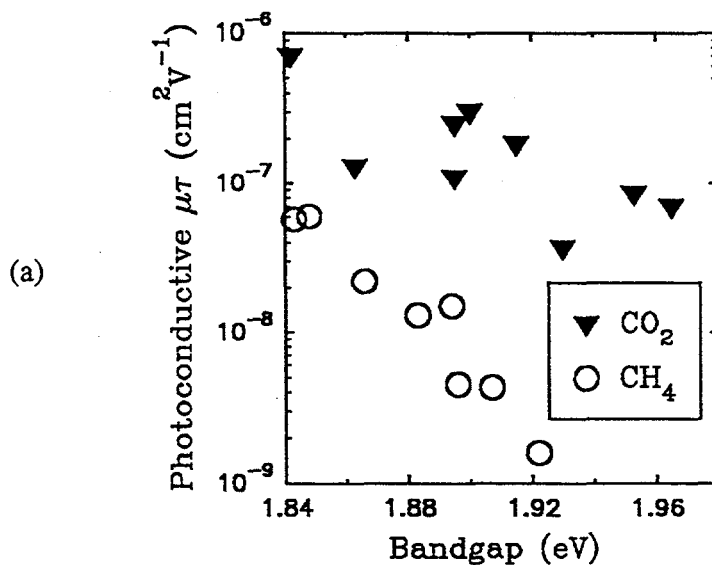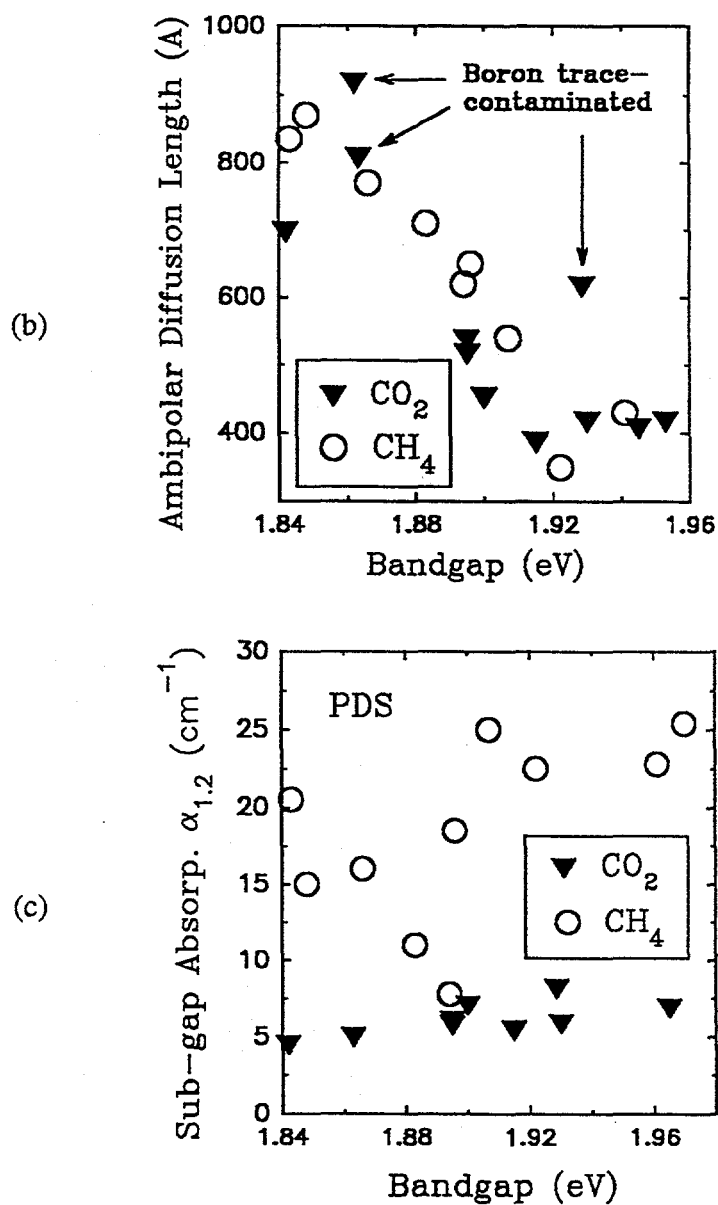
Figure 2-4. Transport and optically active defect data for a-SiO:H and a-SiC:H films: a) photoconductive $\mu\tau$ product, b) ambipolar diffusion length, and c) sub-bandgap absorption at 1.2 eV.

is found to be slightly n-type, as inferred from its higher dark conductivity and lower activation energy as compared with a-SiC:H alloys of comparable bandgaps.

The properties of a-SiO:H p-layers have also been evaluated and were found not to be no better than conventional a-SiC:H p-layers. Similarly, the performance of the single junction p-i-n solar cells having a-SiO:H p-layers are also just comparable to standard a-SiC:H p-layer devices. The device results are summarized in **Table 2-3**.

Table 2-3. Representative Parameters of Simple p-i-n Cells Using CO_2 in the p-layer.

Cell I.D.	p-layer Type	QE @ 400 nm	V_{oc} (V)	J_{sc} (mA/cm^2)	FF	Eff.
S20113H	CH_4	0.64	0.82	15.2	69.6	8.67
S20114J	CH_4	0.64 - 0.67	0.837	15.35	69.9	9.00
S20127U	$CO_2(+H_2)$	0.69	0.843	15.3	67.8	8.74
S20117T	CO_2	0.65 / 0.66	0.845	14.7	69.6	8.63
S20122A	CO_2	0.72	0.803	15.62	69.1	8.67
S20122Z	CO_2, CH_4	0.71	0.829	15.69	68.0	8.84
S20123F	CO_2, CH_4	0.67	0.838	15.32	68.7	8.75
S20124J	CO_2+CH_4	0.73?	0.821	15.81	66.3	8.61
S20130X	CO_2+CH_4	0.64	0.826	15.58	68.0	8.75
S20123G	CH_4	0.68	0.835	15.50	68.6	8.88
S20110A	CH_4	0.68?	0.834	15.72	70.8	9.28
S20128S	CO_2, CH_4	0.66	0.827	15.54	71.5	9.19

Notes: The i-layer thickness is about 3200Å-3500Å (cell non-uniformity and run-to-run variation).

2.2.3 Microcrystalline Si *p*-layer

Although microcrystalline films are, in principle, a means to obtain higher V_{oc}, we have encountered several problems with its use in devices. These are: (1) nucleation of crystalline sites only takes place after the film exceeds a certain minimum thickness (usually >500Å), below which the film remains amorphous; (2) nucleation depends on the substrate which is different for the films prepared for characterization purposes compared to those used for solar cells; (3) adding carbon destroys the microcrystallinity even for thick films. Despite all these difficulties, we have further investigated the growth of microcrystalline material in this period in view of its high potential for improving the device performance. In searching for deposition conditions which would enable us to make thin μc-Si *p*-layers (<500Å), we found that lower substrate temperature helps the formation of the microcrystalline phase. **Table 2-4** lists the properties and deposition conditions of several films prepared for study. Note that the sample made at 180°C has a very high conductivity and low activation energy, characteristic of a microcrystalline doped films. Raman scattering measurements confirmed that this film indeed contains a high volume fraction of the microcrystalline phase. We have incorporated this μc-Si *p*-layer in single junction solar cells and achieved V_{oc} values as high as 0.87V. While this voltage is relatively high considering that there is no carbon in the *p*-layer, even higher V_{oc} (>0.95V) are required for triple-junction devices. V_{oc} values in this range are obtained with conventional a-SiC:H *p*-layers. Moreover, the short wavelength QE of the cells incorporating such μc-Si *p*-layers has been generally low, presumbly due to poorer optical transmission in the μc-Si *p*-layer at short wavelengths.

Table 2-4. Microcrystalline p-Si Film Properties.

Sample #	d.c. curr. (mA)	P (mTorr)	H dil ratio	T (C)	dep. rate (Å/s)	d (Å)	σ_d $(\Omega \cdot cm)^{-1}$	E_a (eV)
D1115-2	900	2,000	50:1	260	2.4	1,200	2.43e-4	0.39
D1118-2	300	2,000	100:1	260	0.35	350	3.93e-4	0.37
D1119-2	300	1,000	100:1	260	0.2	300	3.32e-4	0.11
D1124-2	300	1,000	100:1	245	0.17	500	1.74e-2	0.12
D1126-2	300	1,000	100:1	220	0.17	300	0.54	0.07
D1122-1	300	1,000	100:1	180	0.17	500	1.30	0.04
D1122-2	300	1,000	100:1	130	0.17	350	1.06e-6	0.37

Notes: Total flow rate was ~400 sccm in all cases. Microcrystallinity was confirmed by Raman scattering for films with a large conductivity and a small activation energy.

2.2.4 Microcrystalline SiC

Ganguly, et al. (8) have reported that highly conductive and transparent µc-SiC, both intrinsic and doped, can be made rather easily with the fluorinated feedstocks, $SiF_4 + CF_4$. In this method, only a small amount of H_2 (~10%) was employed, perhaps for the purpose of modifying the surface chemistry during film growth, rather than as a diluent as used in the conventional method of making microcrystalline material. No device results, however, have been reported using such a material. We have begun a study to follow up this new developement and hopefully to demonstrate the usefullness of this material in devices. Our initial results showed that films of very different characteristics, from highly conductive films with dark carbon-like appearence to highly insulating and transparent films, can all be deposited with only small variations in the deposition conditions. We obtained no evidence to suggest that the highly conducting films were microcrystalline; in fact, all highly conducting films had an appearance that indicated a graphitic nature. However, at present we do not have the capability to characterize whether the material is microcrystalline, because Raman spectra of SiC materials are generally buried in the large photoluminescence background. The access of other characterization tools such as electron defraction or TEM would be necessary for a definitive resolution of the question.

2.3 Cell Degradation Under Electrical Bias

A number of kinetic models for light induced defect generation in a-Si:H have been equally successful in explaining most of the experimental data to date, although they were derived from rather different physical mechanisms. Stutzmann, et al. (9) were the first to derive the comprehensive kinetic description based on a bimolecular recombination mechanism in which the non-radiative tail-to-tail recombination is the rate limiting step for defect formation. More recently, Redfield and his coworkers (10) demonstrated that introducing a time dependent "dispersive" prefactor in the rate equation mechanisms based on monomolecular recombination or charge trapping (11,12) could also give rise to the same kinetic behavior as exhibited in the experiments.

The kinetics of light induced degradation of a-Si:H based p-i-n solar cells held at V_{oc} values have been relatively well studied (13). We report here a study on the degradation of a-Si:H solar cells under electrical bias. It is shown that the quantitative comparison of the kinetics of cells degraded at V_{oc} as a function of light intensity with those at various electrical biases but constant light intensity is quite interesting and sheds much light on the validity of several widely discussed models.

The degradation time dependences of a-Si:H solar cells under a wide range of electrical bias from V_{oc} to -4V reverse bias were measured at one sun illumination intensity (100 mW/cm^2). An Oriel solar simulator capable of illuminating uniformly over an area greater than 5 in. in diameter was used as the degradation light source. The light intensity variation during the entire soaking period (~300 hrs) was less than ~5%. The single junction a-Si:H p-i-n solar cells used in this study were made by d.c. glow discharge at 260°C. The thickness of the i-layer was approximately 6000Å. Small area (~0.26 cm^2) diodes fabricated on the same 3 in. x 3 in. glass substrate were held under various bias levels and light-soaked at the same time. The initial cell efficiency was approximately 9.2% before light-soaking. The J-V curve as well as the other device parameters are shown in **Figure 2-5**. The cell temperature during light-soaking was controlled at ~45°C by continuously blowing air to the sample. The electrical bias on the cells during light-soaking were maintained either at a constant voltage or constant current. In the case of constant voltage, the current density slowly decreased with time due to light induced degradation. As a result, the total recombination rate in the cell, which is equal to the total carrier generation subtracted by the charge collection, slowly increased with time. While the total recombination rate was fixed in the case of constant current, the bias voltage was slightly varying. Nevertheless, the differences in the degradation time dependences between the two cases were relatively insignificant with regard to the main conclusions of the paper.
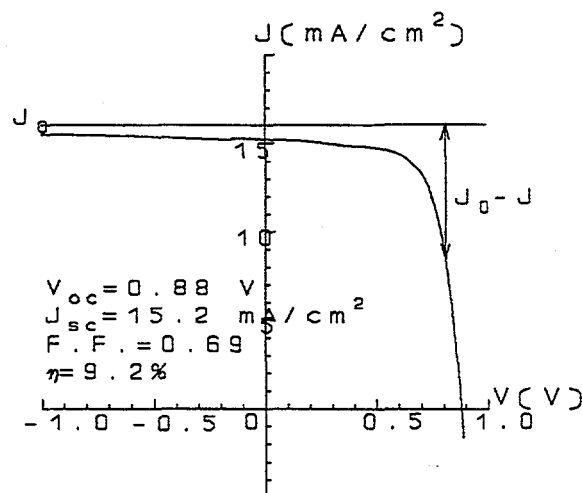
Figure 2-5. The J-V characteristics of the *p-i-n* device. J_0 is the saturated current density at large reverse bias.

It has been demonstrated convincingly **(13)** that the degradation of solar cells under open-circuit condition as well as that of the film properties obeys a simple scaling rule between the light intensity (I) and the illumination time (t) at which the degradation reaches a certain level, i.e.,

$$I^{\alpha} t = \text{const} \tag{1}$$

where the exponent α is around 1.8. It has also been demonstrated (14,15) that the degradation of solar cells is quite insensitive to the wavelength of the light which indicates that the spatial distribution of defect states is relatively unimportant as compared to the integrated defect density. The total recombination rate in the solar cell at V_{oc} or in the film is simply equal to the carrier generation rate and thus proportional to the light intensity. If re-combination is responsible for defect creation, it could be anticipated that the degradation of solar cells would be significantly reduced by collecting photogenerated carriers before the recombination takes place. **Figure 2-6(a)** shows the time dependences of solar cells degradated under various electrical bias. In this set of measurements, the current densities were fixed at constant levels, and hence the recombination rates, for individual cells during the entire course of light-soaking. The data clearly illustrated the general trend that external charge collection reduces the rate of degradation in a-Si:H solar cells. However, it is interesting to compare the experimental results shown in **Figure 2-6(a)** with various defect creation models.
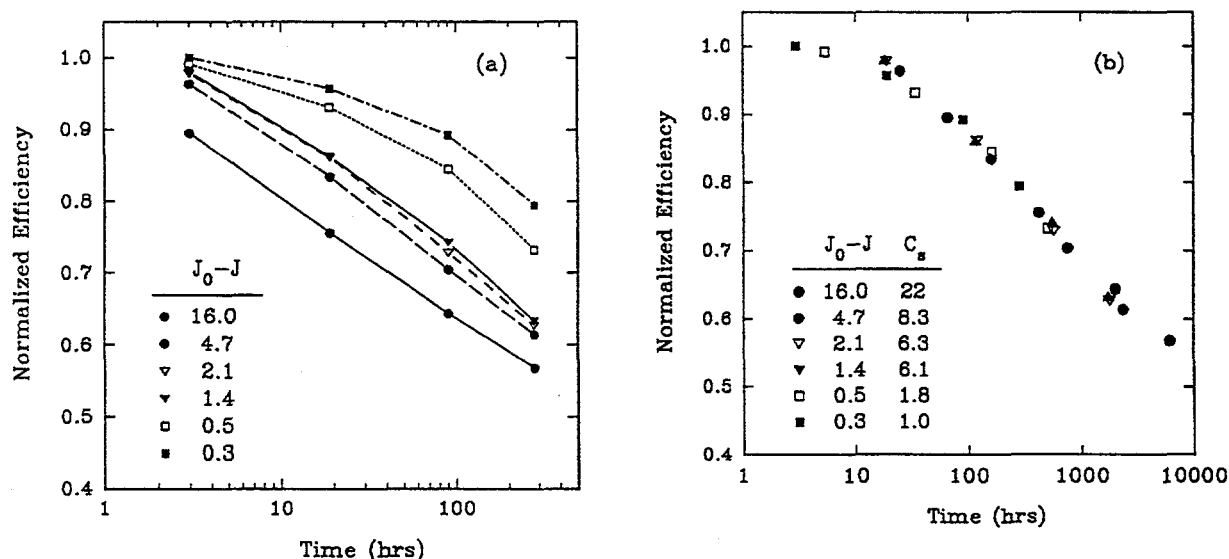
Figure 2-6. Normalized efficiencies vs. light-soaking time for cells held at constant current levels (a). These time dependences are then scaled to the one held at J=0.3 mA/cm^2 using Equation 2 (b).

Since the degradation time dependences shown in **Figure 2-6(a)** have similar functional forms, they can be scaled to the same curve by adjusting the time variable, i.e.,

$$C_s \, t = const. \tag{2}$$

where C_s is the scaling factor. **Figure 2-6(b)** shows the same time dependences as in **Figure 2-6(a)** after scaling to the curve measured with the strongest reverse bias. The scaling factors, which can be used as a measure of the rate of degradation under various bias, are also listed in the figure. On the other hand, the total recombination rate in the device at a constant current level (J) is simply equal to $(J_0 - J)/e$, where e is the electron charge and J_0 is the saturated current density at very large reverse bias. We have plotted the scaling factor C_s listed in **Figure 2-6(b)** versus $(J_0 - J)$ in **Figure 2-7**. If the rate of defect formation is directly proportional to the total recombination rate, as often perceived (**16**), the light intensity scaling rule under the open-circuit condition, Eq. 1, would predict that with increasing J the scaling factor C_s decreases as $(J_0 - J)^{1.8}$. As shown by the solid curve in **Figure 2-7**, this scaling rule clearly gives a much faster reduction in degradation than experimentally observed. We note that our experimental data on the bias dependence of solar cell degradation are in general agreement with the earlier results (**17,18**). However, the interpretation given by Nakata et al. (**18**) was somewhat misleading. In the following, we compare in detail the kinetic behavior of solar cell degradation under both open-circuit condition and electrical bias to various defect creation models. We assume that only one degradation mechanism is operational in the device with and without electrical bias.
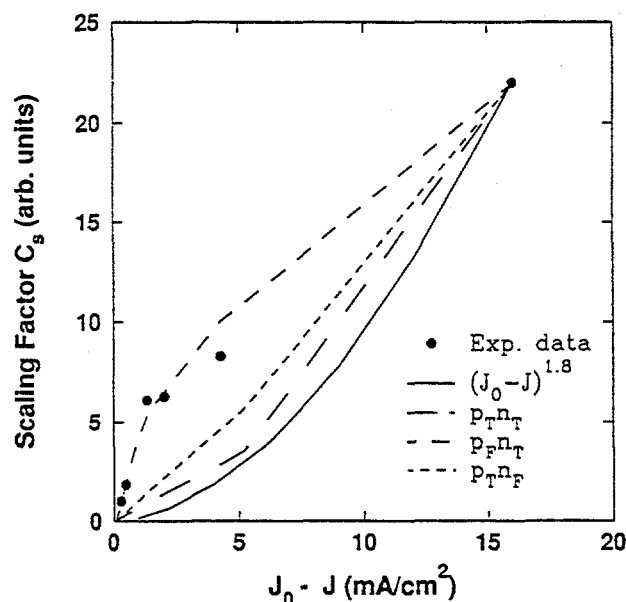
Figure 2-7. Scaling factor C_s vs. the total recombination rate, $J_0 - J$. The curves are calculated based on various models.

2.3.1 Monomolecular Recombination

Although the energy released from monomolecular recombination through midgap defect states is generally considered too small for bond breaking, it may be sufficient to allow the bonded H to hop and insert into a neighboring Si-Si weak bond (19), or to assist reconfiguration after a carrier being trapped by the charged defect. Since recombination at the present generation rate is predominantly monomolecular through midgap defect states, the bias dependence of monomolecular recombination would be the same as the total recombination. Therefore, any defect creation model in which monomolecular recombination is the dominant rate limiting step would also be inconsistent with the experimental results shown in **Figure 2-7**.

2.3.2 Bimolecular Recombination

While any form of bimolecular recombination could be compatible with the light intensity dependence for films and solar cells at open-circuit (9), Stutzmann (20) suggested that the "weak" Si-Si bond is likely to be broken by the recombination of an electron hole trapped at the same "weak" bond site forming an exciton. The attractiveness of this version of bimolecular recombination model is the localization of both carriers which is essential for concentrating the recombination energy leading to bond breaking. Assuming that the probability for forming such an exciton is proportional to the product of trapped electron and hole densities in the respective band tails, the recombination rate responsible for the defect formation is then proportional to the integral of $p_T n_T$, where the subscript T denotes trapped carriers in the tail states.

Since it is not straightforward to estimate the bias dependence of the carrier densities across the i-layer in a solar cell, we have employed the well established device modelling facility at Penn State University (21) to derive the bias dependence for this integral. Numerical simulations were carried out for solar cells operating under various bias levels. The long dashed curve in **Figure 2-7** shows the integral of $p_T n_T$ versus the total recombination rate in the i-layer, which was normalized to the data at V_{oc}. It is apparent that this channel of bimolecular recombination has a bias dependence close to $(J_0 - J)^{1.8}$, and thus is also inconsistent with the experimental observation.

We have further explored possibilities of other channels of bimolecular recombination using the computer simulation. Two of the remaining channels which have some degree of charge localization are the recombination between a free hole and a trapped electron ($p_F n_T$) and between a free electron and a trapped hole ($p_T n_F$), where subscript F denotes free carriers. In **Figure 2-7**, the short dashed curve shows the computer simulated bias dependence for the integral of $p_F n_T$ and the dotted curve for the integral of $p_T n_F$, respectively. While the bias dependence of $p_T n_F$ is

16

again substantially different, that of $p_F n_T$ is almost identical to what was observed experimentally. The results shown in **Figure 2-7** strongly indicate that the recombination between a free hole and a trapped electron is the only recombination mechanism that could be consistent with the degradation kinetics under both open-circuit condition and electrical bias. It should be pointed out that the magnitude of $p_F n_T$ is much smaller than that of $p_T n_F$. Therefore, if carrier recombination is indeed the mechanism for defect formation, an asymmetry in terms of defect creation must exist between the two recombination channels.

If the free carrier does form an exciton with the trapped carrier having opposite charge, it is conceivable that the size of the exciton formed by a free hole with a trapped electron is substantially smaller than that of the exciton formed by a trapped hole with a free electron. This is because the size of an exciton is inversely proportional to the effective mass of the free carrier which could be over an order of magnitude larger for the free hole than for the free electron **(22)**. Therefore, the recombination of a free hole with a trapped electron might provide the necessary localization to break the "weak" Si-Si bond and form the defect. It should be pointed out that this mechanism does not exclude the possibility that the recombination of the electron-hole pair trapped at the same "weak" bond site could also create defects, but its probability may be too small to have any effect on the kinetics.

It has been difficult for the recombination models to explain the metastability induced by single carrier injection which, on the other hand, has been considered as one of the main supporting evidences for the charge trapping model **(11)**. However, it has been shown experimentally that significant defect generation occurs only by single carrier injection of holes in the p-i-p structure, but not by injection of electrons in the n-i-n structure **(23)**. This asymmetry can, in principle, be explained by the $p_F n_T$ recombination mechanism because the injection of holes, which have a much lower equilibrium density than the electrons, would significantly increase the $p_F n_T$ recombination rate, but the injection of electrons would not.

While the above discussion is based specifically on the "weak" Si-Si bond breaking model, it can be extended to any other models which involve bimolecular recombination as the rate limiting step, including possibly the light induced H redistribution model **(19,20)**. It should also be noted that although the Penn State computer model **(21)** has been successful in describing the solar cell operation, its accuracy in describing the above microscopic processes remains to be fully established.

2.3.3 Charge Trapping

The charge trapping model for defect creation is based on the concept that charged defects do exist in undoped a-Si:H, at least in some regions, and that by trapping a carrier they could reconfigure into a metastable neutral defect state (11). Thus, the creation rate for the neutral defects in this case would be proportional to the product of the carrier density and the charged defect density. In p-i-n solar cells, it is expected that additional charged defects exist near the interfaces due to space charge accumulation. However, the density of the carrier with opposite charge are normally substantially lower in the interface regions. Since the electrical bias not only affects the spatial distribution of the carrier densities in the i-layer, but also that of the charged defects which is largely unknown, a quantitative analysis on the degradation of solar cells under electrical bias is thus complicated. The analysis of the other similar model based on the RTS (*R*ehybridized *T*wo-*S*ite) center (12) can in principle suffer from the same complication. There-fore, the present experiment is not well suited for examining the validity of such models.

In conclusion, we have clearly demonstrated that charge collection under electrical bias improves the stability of a-Si:H solar cells. However, the quantitative results are not consistent with the model that the rate of defect generation is directly proportional to the total recombination rate. Numerical device simulation suggests that the bimolecular recombination between a free hole and a trapped electron could be the mechanism for defect creation through either Si-Si bond breaking or H redistribution. A comparable discussion on the charge trapping model cannot be carried out in this context due to lack of detailed understanding on the possible bias effect on the charge defects.

3.0 TASK II: NON-SEMICONDUCTOR MATERIALS RESEARCH

The purpose of this task is to develop contacts which permit improved optical efficiency of triple-junction superstrate devices. Our primary emphasis in this task has been to develop ZnO with very high optical transmission.

3.1 APCVD of ZnO

Although textured SnO_2 is currently used as a front contact layer for solar cells and modules, optical analysis of the amorphous silicon multijunction structure indicates that the present SnO_2 material used in the solar cell front contact accounts for significant (8%-10%) optical losses. Efforts to reduce these optical losses centered around minimizing optical absorption and increasing light scattering while improving the electrical conductivity of the transparent front contact by employing ZnO.

ZnO films offer several advantages over SnO_2 as a front contact. A lower optical absorption in the blue region of the visible spectra is expected from ZnO films because of a larger bandgap (24) (3.2 eV) compared with the bandgap obtained with SnO_2 films (3.0 eV). Doped ZnO films can be prepared with high conductivities using such dopants as fluorine, aluminum, or boron. In addition, ZnO is more resistant to reduction by the hydrogen plasma encountered during a-Si:H depositions. Thus, it should be possible to produce a more optically transparent window in devices built on a ZnO film using hydrogen dilution. Furthermore, ZnO is more easily etched with dilute acid making equipment maintenance easier and the by-products are non-corrosive - also reducing maintenance costs. Conversely, the greater "softness" of the ZnO films may give rise to handling problems. Lastly, the waste products of ZnO deposition are less toxic and do not require as much scrubbing and treatment as those from SnO_2 deposition.

ZnO can be prepared by LPCVD, APCVD, spray pyrolysis, sputtering, and a number of other methods (25). The chief advantage of APCVD of ZnO is that it would utilize the existing equipment employed for SnO_2 deposition and be amenable to continuous processing. By operating at atmospheric conditions, no complex vacuum systems are needed such as are required for LPCVD of ZnO. As we will see later, different deposition techniques produce ZnO with far different properties. APCVD ZnO has excellent optical and electrical properties for a front contact in a-Si:H and other thin film photovoltaic devices.

APCVD of ZnO was carried out in a Watkins-Johnson furnace, whose facilitation was completed during this reporting period. Depositions were carried out on 3 in. x 3 in. pieces of Corning

7059 glass. As indicated in **Figure 3-1**, the furnace carries substrates on a moving belt through the furnace in a nitrogen atmosphere, under the deposition heads, producing the conducting film. Movement of the substrate during APCVD of ZnO was found to be necessary based on initial studies with a deposition system that had a static substrate. In that study, it was found that in a wide range of ZnO deposition conditions it was not possible to obtain films with uniform optical and electrical properties using atmospheric deposition when the substrate remained in a fixed position. The inability to prepare uniform ZnO samples at atmospheric pressure without sample movement is related to the rate of diffusion of reactants to the substrate surface. In contrast, in LPCVD (pressures of 1-50 torr) of ZnO, the low pressure permits rapid gas phase diffusion of reactants; hence, batch system with immobile substrates yield uniform films.

INJECTOR #1   INJECTOR #2   INJECTOR #3
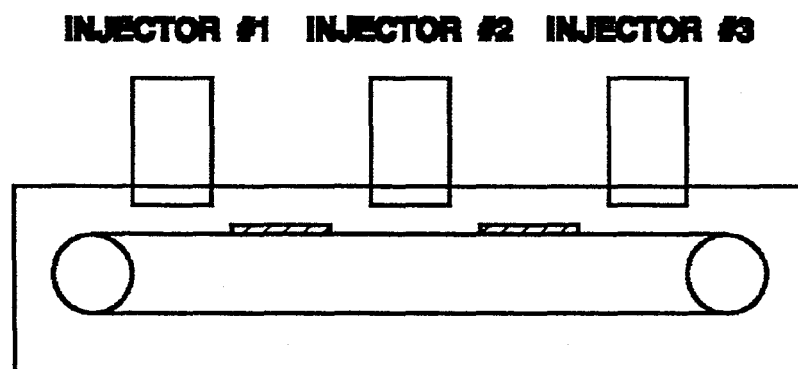
Figure 3-1. Picture of the APCVD furnace showing how glass substrates are moved under the injection heads.

The zinc source for the APCVD furnace is the commercially available pyrophoric liquid (boiling point 118°C) DEZ that is thermally stable in the absence of air. A number of oxygen containing compounds (H_2O, O_2, N_2O, methanol, tertbutyl alcohol, etc.) (**26**) have been reported in the literature to react with DEZ to give ZnO films. The best results for atmospheric deposition of ZnO have been obtained with anhydrous ethanol (**27**). The reaction between DEZ and ethanol is given by:

$$Zn(CH_2CH_3)_2 + CH_3CH_2OH ---->ZnO + C_2H_4 + 2C_2H_6$$
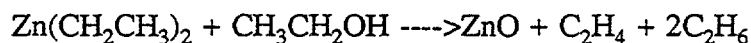
In practice, the process of film formation is conducted by combining gaseous DEZ and gaseous ethanol in a deposition head supplied by metal bubblers heated to above room temperature. The bubblers were fed a nitrogen carrier gas through a mass flow controller with the precise level of DEZ and ethanol determined by the bubbler temperature and the vapor pressure of the liquid. The reactant lines were heated to above the bubbler temperature to ensure that no liquid condensed in the lines. In addition to the main reactants, trace amounts of water vapor were added to ethanol vapor to improve film properties.

20

The major variables, such as oven temperature, dopant flow, DEZ flow, water vapor flow, diluent nitrogen flow rates, exhaust rate, and belt speed were examined to optimize uniformity, conductivity, and transmission. To obtain sufficiently thick films (0.3 - 1.0 μm), a belt speed of 3 in. to 6 in. per minute was used. **Figure 3-2** shows the temperature profile of the center portion of furnace that was obtained by attaching a thermocouple to a glass substrate and sending the substrate through the furnace at 600°C on the belt. The ZnO deposition is clearly not isothermal. The substrate experiences a drop of up to 100°C when it passes under the deposition heads with their cooling flow reagents and nitrogen. Between injectors the furnace is able to reheat the substrate.
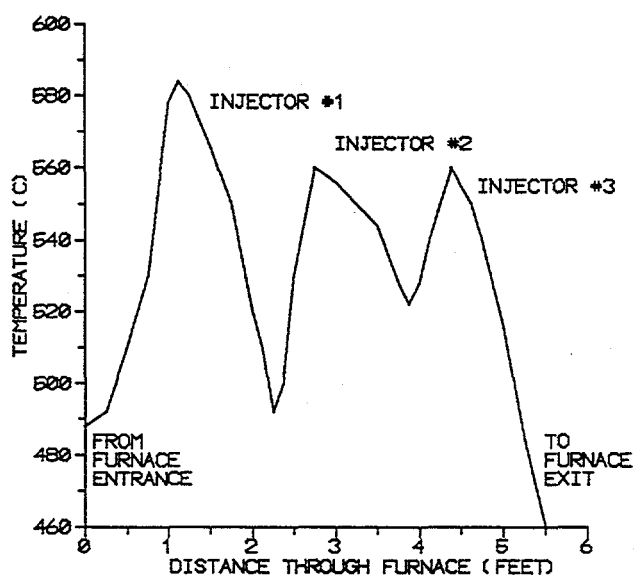
Figure 3-2. Temperature profile of the center of the APCVD ZnO furnace made by passing a glass substrate with a thermocouple attached through the furnace at 6 in. per min. The furnace was set at 600°C. The dips in temperature indicate the location of deposition heads. There is no further heating after the third injector.

In early experiments, there was a tendency for the head to become clogged by ZnO powder. This was eliminated by careful adjustment of the exhaust and reactant flows. It was necessary to permit the furnace to stabilize at a given set of conditions prior to sample preparation in order to obtain satisfactory reproducibility. Some measure of the reproducibility of the films can be seen in **Figure 3-3** by noting the changes in conductivity from a series of twelve samples prepared consecutively. **Figure 3-4** shows the changes in transmission and haze for the same samples. In both figures the vertical lines show the range of data with the connecting lines running through the midpoint of the range. Some measure of the present uniformity of larger area ZnO films can be obtained from **Figure 3-5** which shows the resistance, optical transmission, and haze for a 6 in. x 12 in. sample of glass taken at 8 different points.

21
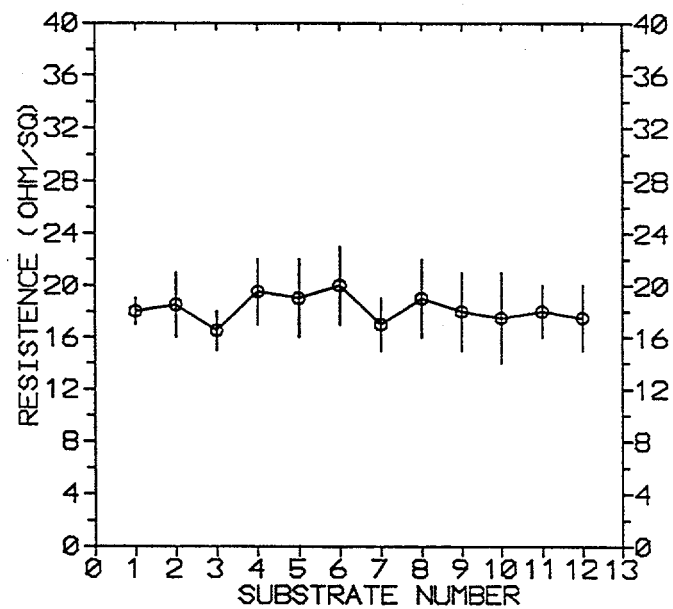
Figure 3-3. Resistance of 12 fluorine doped ZnO films (0.7 μm thick) on 3 in. x 3 in. glass substrates deposited sequentally showing reproducability. Vertical lines indicate range of readings.
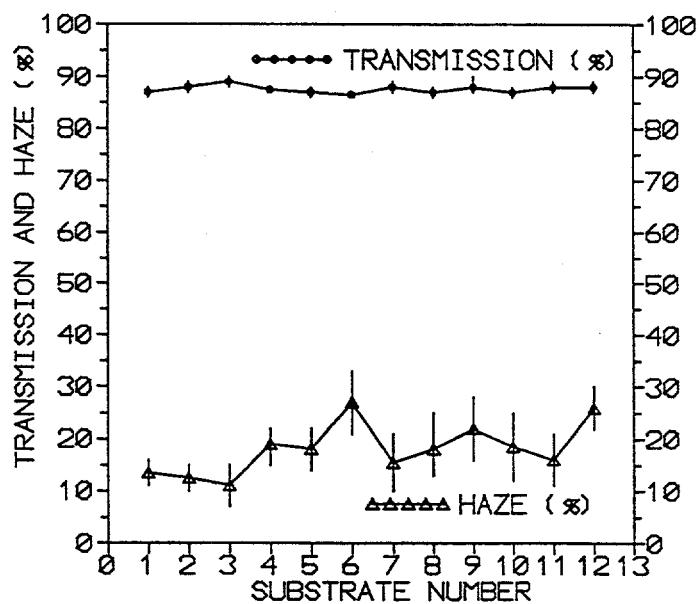
Figure 3-4. Transmission and haze of twelve fluorine doped ZnO films whose resistances are reported in **Figure 3-3.**

10 ohm/sq	9 ohm/sq
80% transmission	84% transmission
37% haze	29% haze
11 ohm/sq	12 ohm/sq
80% transmission	84% transmission
38% haze	29% haze
9 ohm/sq	11 ohm/sq
81% transmission	85% transmission
39% haze	29% haze
9 ohm/sq	12 ohm/sq
83% transmission	84% transmission
31% haze	28% haze

Figure 3-5. Resistance, transmision, and haze of ZnO on a 6 in. x 12 in. module size glass substrate demonstrating uniformity across a large substrate. Note that the Hazeguard hazemeter used to measure transmission under-estimated the actual transmission.

Table 3-1 gives a list of the properties of selected APCVD ZnO films. For comparison, typical SnO_2 and LPCVD film properties are included. **Figure 3-6** shows the visible spectum in air of a matched pair of ZnO and SnO_2 samples with similar resistances and hazes. **Figure 3-7** shows the visible spectra of the same two samples run in a high index fluid (diiodomethane) which reduces the amount of light scattered out of the optical path of the spectrometer thus giving a "true" measure of the optical transmission. The difference in the transmissions recorded in **Figures 3-6** and **3-7** is due to the increased light scattering out of the optical path when the sample is measured in air. The results clearly show that the ZnO absorbs less light confirming that ZnO films are optically superior to similar SnO_2 films. ZnO surface roughness was characterized by a Dektak IIA Surface Probe Measuring System, (Veeco/Sloan Technology, Santa Barbara, CA). The optical haze and transmission values were obtained using a Gardner (Silver Springs, Maryland) Hazegard hazemeter which yield an average value over the visible spectrum.

Table 3-1. Properties of a Variety of ZnO and SnO$_2$ Films.

Film Type	APCVD ZnO	APCVD ZnO	LPCVD ZnO	LPCVD ZnO	Sputtered ZnO	APCVD SnO$_2$
Thickness (Å)	5,500	7,000	8,500	15,000	800	9,000
Resistance (Ohm/Sq.)	11-13	18-22	12-15	5-6	320	15-25
Transmission (%)	89	84-86	87.0	82.0	88-92	78-92
Haze (%)	5-6	14-18	2	12	0-1	20-30
Dopant	C$_3$F$_6$	C$_3$F$_6$	B$_2$H$_6$	B$_2$H$_6$	Al	HF

Initially, the samples were non-uniform and it was difficult to optimize depositions when the films contained materials with a wide range of optical and electrical properties. The major improvements in uniformity were accomplished by altering the position of the head to prevent turbulent flow. Uniformity also appeared to improve by switching from hydrogen fluoride (0.5% HF in nitrogen) to hexafluoropropylene (C$_3$F$_6$, HFP). The decompositon of HFP produces fluorine doping of the oxide. As indicated in **Figure 3-8**, at high HFP flows, no further improvement in conductivity is obtained. This suggests that the kinetics of decompositon of the HFP limits the availability of fluorine. Studies with HF indicate a clear maximum conductivity established by the incorporated F.
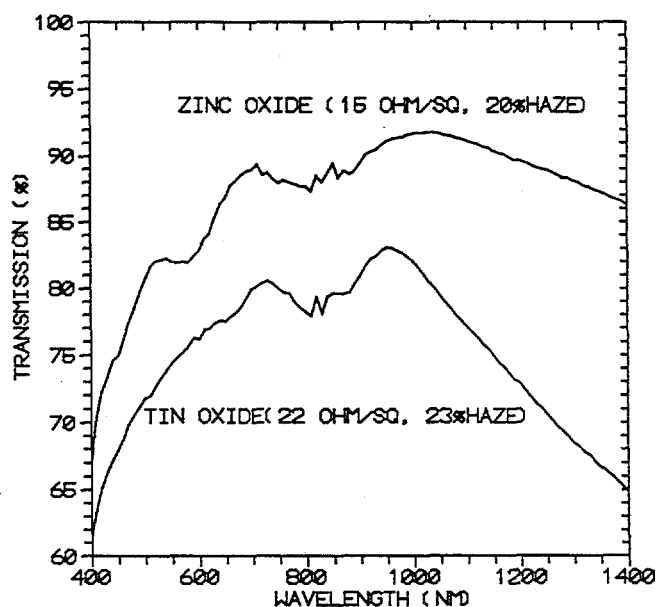
Figure 3-6. Comparison of the visible spectrum of matched ZnO and SnO$_2$ films with similar resistances and hazes run in air. (Irregularities at 860 nm caused by detector change).

24
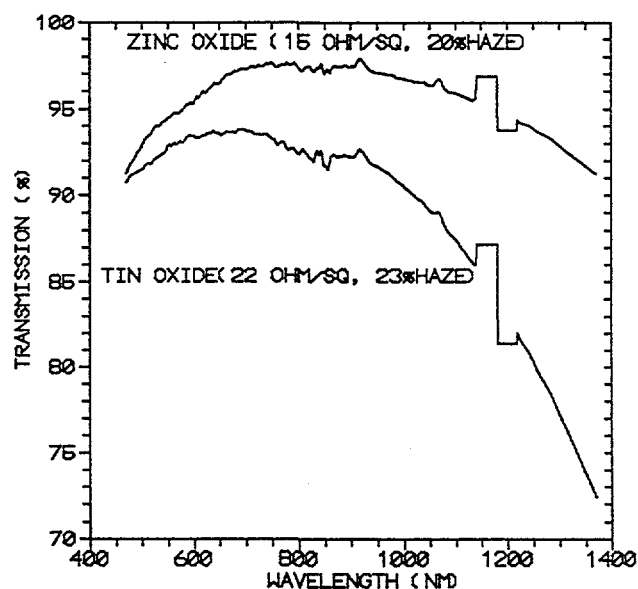
Figure 3-7. Comparision of the visible spectrum of matched ZnO and SnO$_2$ films with similar resistances and hazes run in a high index fluid (diiodo-methane, index of refraction: 1.749). (Gaps in spectra at 400nm and 1200nm caused by light absorption of solvent. Irregularities at 860nm caused by detector change).
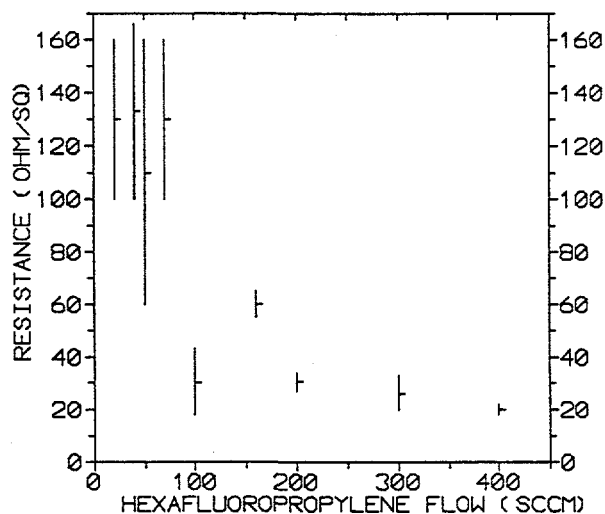
Figure 3-8. Change in resistance of ZnO films as a function of dopant (hexafluoropropylene) flow rate. The films are 0.5 - 0.6 μm in thickness.

Although pressure is not a variable in the APCVD system, the exhaust rate which is inversely related to the reagent residence time must be optimized. **Figure 3-9** shows the effect of adjusting the exhaust rate. Not surprisingly, the film thickness decreases as the exhaust rate increases and the residence time decreases. These results can be interpreted to mean that the longer time re-

agents spend in the furnace, the greater is the chance that they will react and deposit. Surprisingly, better conductivity is obtained at higher exhaust rate, despite the lower film thickness.
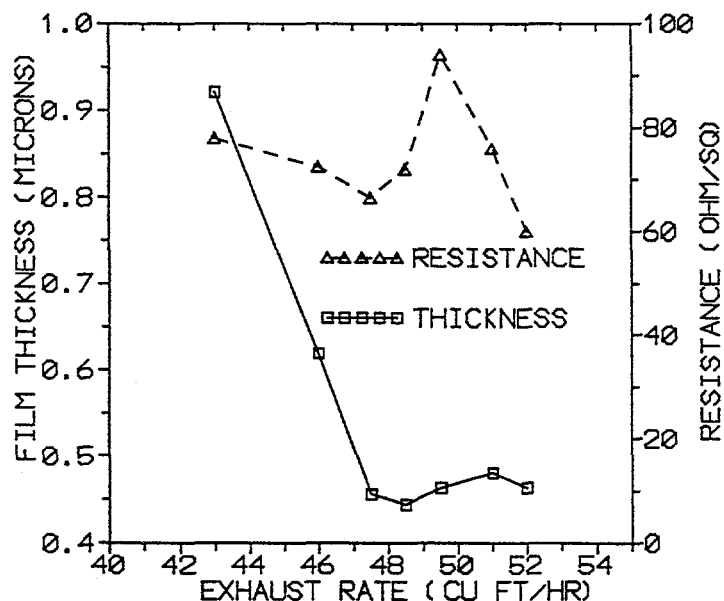
Figure 3-9. Change in APCVD ZnO film thickness and resistance as the exhaust rate from the furnace is increased.

Figure 3-10 shows that the deposition rate is related to the DEZ flow rate. The reaction is run with a very large excess of ethanol (typically 20 to 40 fold excess). **Figure 3-11** shows a graph relating ethanol flow to the properties (thickness, resistance, haze, and transmission) of the ZnO sample. The results clearly show that high ethanol flow rates are necessary to obtain significant haze and high growth rates. The graph demonstrates how haze and transmission are often inversely related. Surprisingly sheet resistance increases as thickness increases. **Figure 3-11** points out the need to optimize haze, transmission, and sheet resistance simultaneously. **Figure 3-12** demonstrates how increasing the water content increases ZnO film uniformity while the haze decreases. Transmission is nearly independent of water content. Clearly the optimum ZnO film represents a compromise between conductivity, transmission, and haze. Interesting insights into the ZnO film structure have come from scanning electron micrographs (SEM) such as those shown in **Figure 3-13**. ZnO prepared by APCVD appears to be made of a large number of spheres that are 0.1 - 0.2 μm in diameter. Large "dust" particles are also visible. In contrast, the LPCVD ZnO is made up of highly crystalline material structure with many pores and crystallites 0.5 - 1.0 μm across that provide a very large surface area. It is clear that APCVD ZnO structurally different material from the highly crystalline LPCVD material.
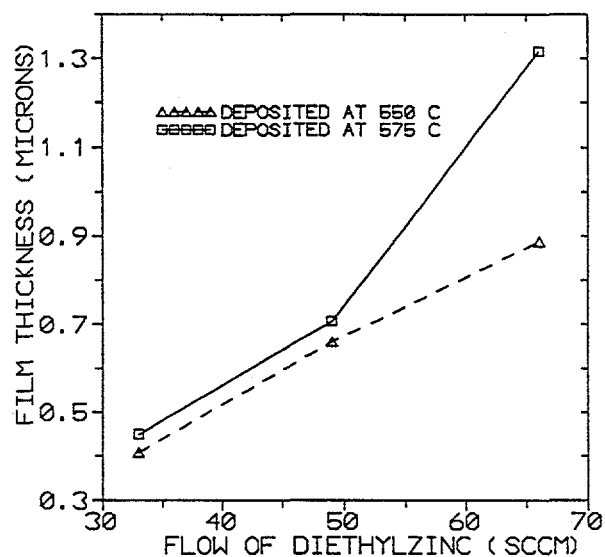
Figure 3-10. Effect of the flow of DEZ on the thickness of APCVD ZnO films.
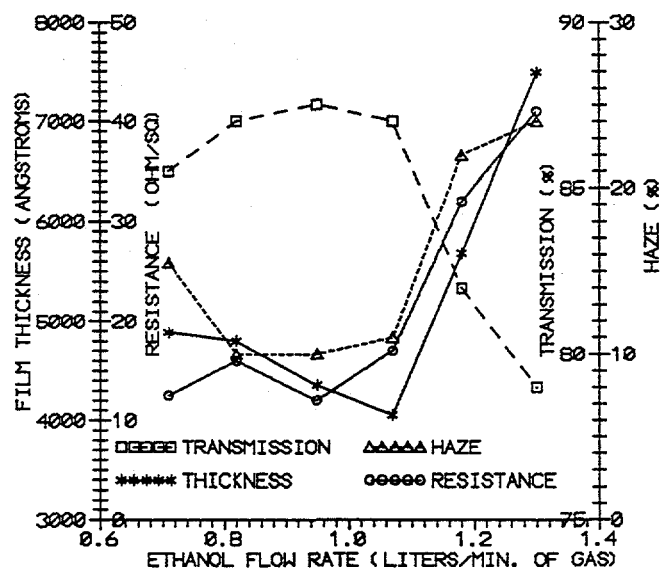
Figure 3-11. Affect of the ethanol flow at 550°C on the thickness, sheet resistance, transmission, and haze of ZnO films. DEZ flow is 50 sccm.

27
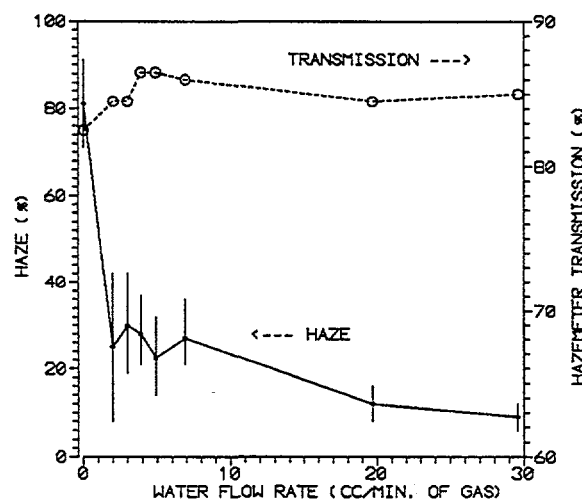
Figure 3-12. Effect of water flow on the optical properties of ZnO. Vertical lines indicate range of measure values.
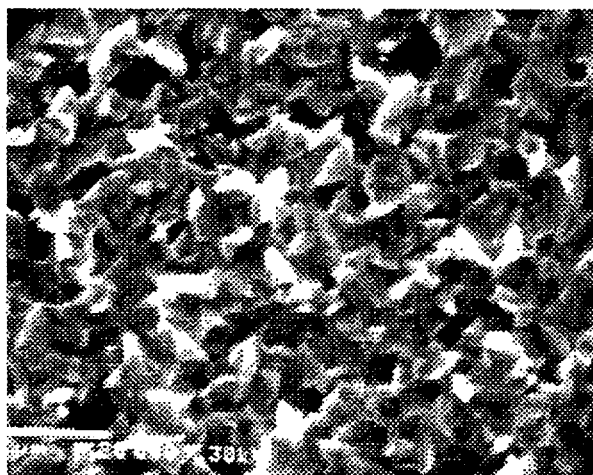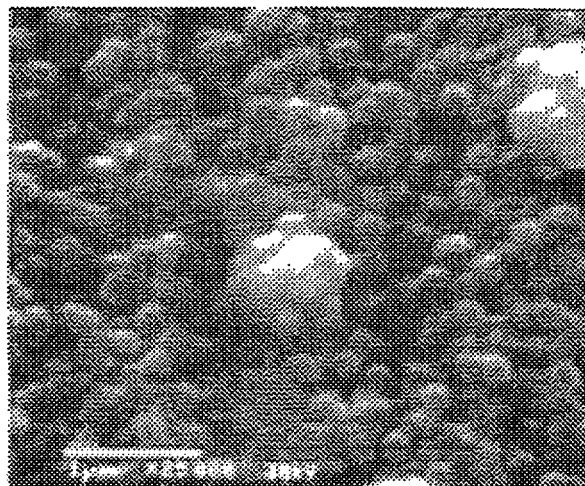
           (a)   (b)

Figure 3-13. SEM pictures showing the difference between the highly crystalline LPCVD ZnO films (a) and the APCVD films of small spheres (b).

3.2   Devices Prepared on ZnO

The improved transmission for ZnO presented in the last section is borne out in measurements of devices prepared on those substrates. **Figure 3-14** presents the QE of a standard single junction p-i-n control device prepared on both the new ZnO and "standard" SnO_2 coated glass substrates. The higher transmission of the ZnO is well demonstrated by the substantially higher

peak QE of devices on ZnO (94%) compared to SnO_2 (85%). This translates into a J_{sc} of 18.9 mA/cm^2 for the devices prepared on ZnO coated glass vs. 16.6 mA/cm^2 on SnO_2 coated glass; an improvement of 2.3 mA/cm^2 or 14%.
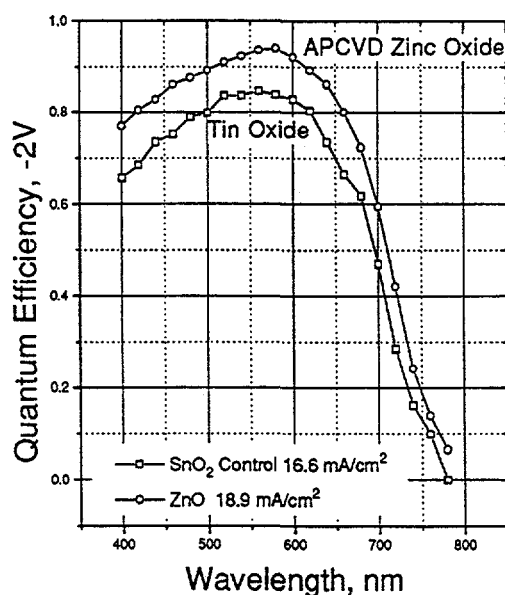
Figure 3-14. Comparison of 6KÅ a-Si:H *p-i-n* devices on ZnO and SnO_2.

Although we have not yet optimized devices on ZnO, the first triple-junction devices have shown excellent performance and gave good reason to be optimistic about eventual improvements in module performance. **Figure 3-15** plots the QE of an a-Si:H/a-Si:H/a-SiGe:H device that contains a 4000Å middle junction i-layer. An efficiency of 11% was measured under our multi-source simulator. The QE of the device is shown in **Figure 3-15**. A peak of QE of 89% is found to be lower, owing to absorption in the first tunnel junction which is of course lacking in the single junction device. **This is the highest performance we have ever measured on thin triple-junction devices.**

The full benefit of the improved current is not translated into an increasing conversion efficiency owing to a higher series resistance usually found with ZnO based devices. In addition, we frequently find lower V_{oc} values on ZnO based devices. Experiments indicate that the high series resistance is due to an increase in the p/ZnO contact resistance. Weller, et al. **(28)**, have suggested that zinc diffuses into the p-region raising the resistivity of that layer. Other experiments have suggested that a pre-treatment of the ZnO with an oxygen glow discharge could lower contact resistance. We fabricated single junction p-i-n devices on ZnO films prepared by both LPCVD and APCVD. We used SnO_2 as a control in each run as well as ZnO that had no

29
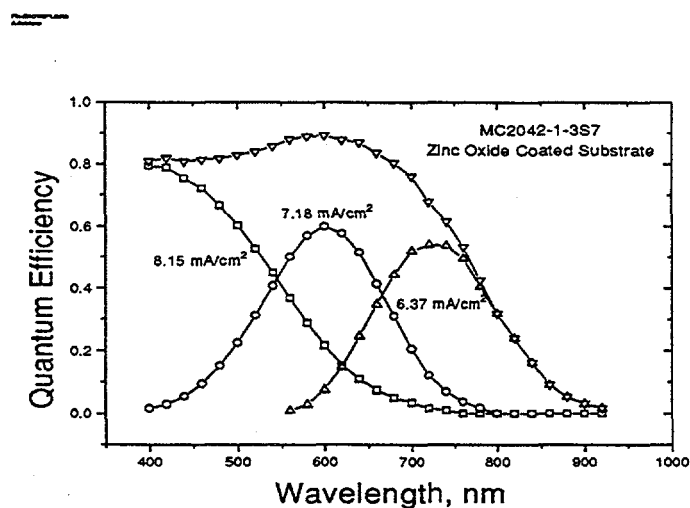
Figure 3-15. QE vs. wavelength for an 11% triple-junction cell prepared on ZnO.

surface treatment. Heating in high vacuum for several hours prior to deposition resulted in no improvement. Likewise, a chemical treatment with hydrazine, a strong reducing agent, did not reduce series resistance. Neither argon nor hydrogen glow discharge resulted in any benefit. An oxygen plasma treatment did have the effect of lowering contact resistance while increasing the V_{oc} of the device, although a small decrease in J_{sc} was noted. It was not immediately apparent if the decrease in current resulted from a reduced light transmission of the oxide. **Figures 3-16 and 3-17** summarize the effect of these treatments on the V_{oc} and series resistance.

In an attempt to reduce the series resistance we also examined the effect of changes in the composition of the p-layer on the series resistance. This data are summarized in **Figure 3-18.** As anticipated, increasing the conductivity of the p-layer by removing carbon, lowers the resistance. Unfortunately the lower transmission of the layer offsets the high optical transmission of the ZnO. If, as has been suggested, the diffusion of zinc into the p-layer is the culprit, then the use of a blocking layer, deposition of the p-layer at lower temperatures or the use of a microcrystalline front contact might solve this problem. Evidence for the benefit of low temperature has been obtained by fabricating devices in a multichamber system in which the p-layer was deposited at 200°C. Those devices gave series resistance values comparable to SnO_2.
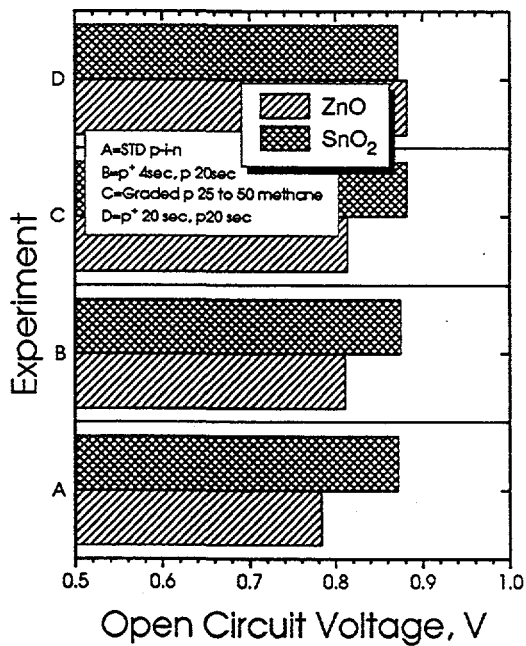
Figure 3-16. V_{oc} of p-i-n devices prepared on ZnO and SnO_2. The p-layers were altered to maximize performance.
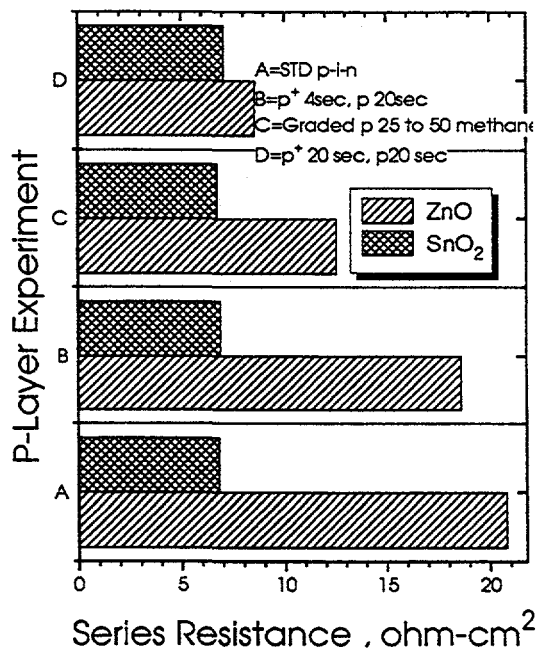
Figure 3-17. Series resistance of p-i-n devices prepared with various p-layer designs as listed in the figure. Both SnO_2 and ZnO coated substrates were used.
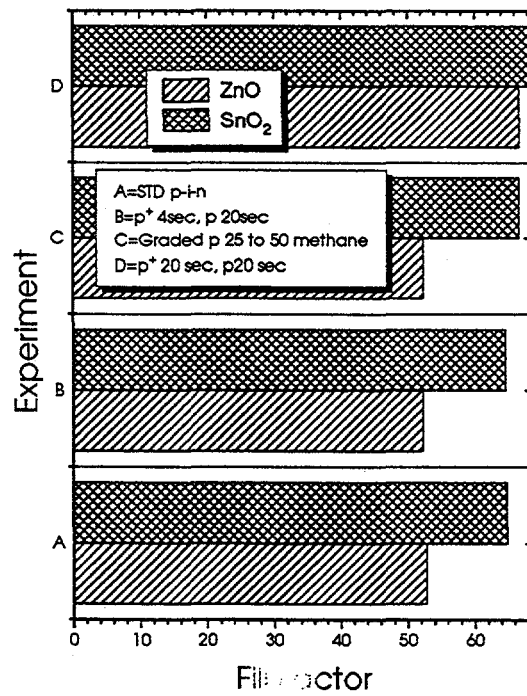
Figure 3-18. Fill factor for various p-layer formulations on SnO_2 and ZnO coated substrates.

4.0 TASK III: MODULE RESEARCH

The goal of the Task III effort in Phase II of the contract is to demonstrate a stabilized module efficiency (600 hrs., AM1.5) of 10.5%. Due to several factors, this goal was not achieved. Among the problems contributing to this has been 1) shunting defects that increase the rate of degradation, 2) the available light sources preventing accurate degradation of modules, and 3) important developments such as the ZnO and a-SiC:H were not ready to be included in the modules. Nonetheless, we have tested modules with initial aperture-area efficiences as high as 10.85%. NREL measured 9.62% and 9.00% indoors and out, respectively. Based on our experience with small area cells, we expect degradation of no more than 20% leading to a stablized efficiency of 8.7%. By incorporating the developments under Tasks I and II (a-SiC:H and ZnO), we expect an increase in the initial module efficiency to the range of 12.5% with little or no increase in degradation.

4.1 Effect of Light Source Spectrum on Module Degradation

We have recently taken steps to address some of the issues which arise when non-ideal light sources are used to degrade solar cells. These problems are always present to some extent when any light source other than the sun is used for light-soaking. However, there is no significant problem when single junction cells are light-soaked as long as the lamp intensity is adjusted so that the current generated by the non-ideal light source is equal to that which would be generated when the cell is under an ideal light source. This is the only correction required for single junction cells because the ability of photons to generate defects does not depend on the wavelength of the incident light. The situation is more complicated for multijunction cells, as the current generated in each component cell will depend on a convolution of the spectral irradiance of the lamp and the QE of each component cell.

A calculation was made of the current which would be generated in each component of a "standard" triple-junction under three different light sources. These light sources were 1) an ideal AM1.5 source, 2) a Na vapor lamp of the type used for degradation studies at Solarex, and 3) a Vortek low pressure argon arc lamp (the lamp used for light-soaking at NREL). Spectral irradiance data for the three lamps is shown in **Figure 4-1**. The Na vapor lamp has a peak near 600 nm, with an additional narrow peak at 820 nm. The Vortek lamp output has a peak irradiance at wavelengths longer than 700 nm. The light absorbed in each junction of a triple-junction cell is therefore very different for each of these light sources. For the cell having the QE shown in **Figure 4-2**, the current density generated in each junction is shown in **Table 4-1**. **Table 4-2**

33

gives the ratio of the current generated in each junction for the Na vapor and Vortek lamps to the current which would be generated using an ideal AM1.5 light source.
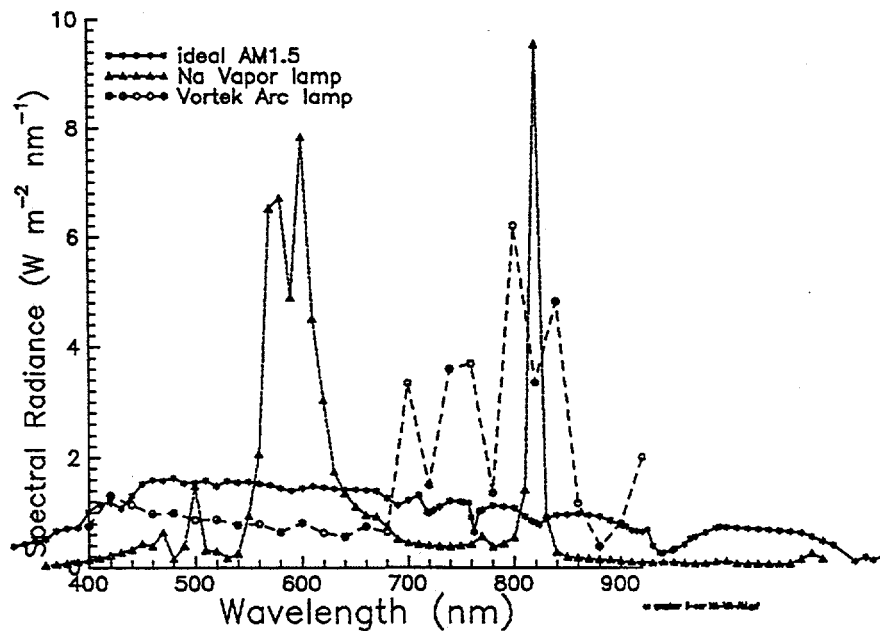
Figure 4-1. Spectral irradiance vs. wavelength for three light sources used for degradation studies.
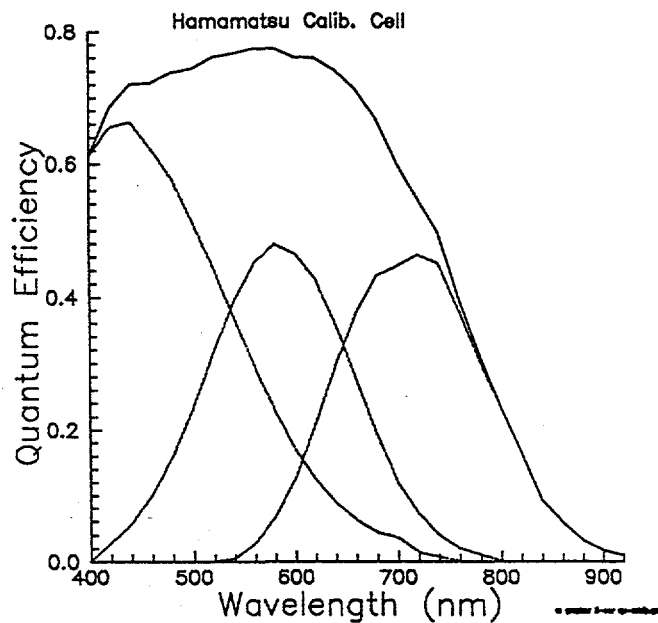
Figure 4-2. QE of a "standard" triple-junction device used in the calculations.

34

Table 4-1. Current Density in Each Component of a "Standard" Triple-Junction Cell for Various Light Sources [mA/cm^2].

Front Cell	Middle Cell	Back Cell	Total	Light Source
5.53	10.84	6.98	23.35	Na vapor lamp
4.13	3.61	11.08	18.82	Vortek arc lamp
6.76	5.74	5.72	18.22	AM1.5

Table 4-2. Ratio of Current Generated in Each Junction for Each Lamp to the Current Which Would Be Generated Under AM1.5 Illumination.

Front Cell	Middle Cell	Back Cell	Lamp
0.82	1.89	1.22	Na vapor
0.61	0.63	1.94	Vortek

Although neither light source illuminates the front cell adequately, this is probably not a serious problem as the front cell in a triple-is very thin and therefore does not degrade at an appreciable rate. More serious problems exist for the middle and rear junction components: the Na vapor lamp has twice the proper amount of light absorbed in the middle cell, while the Vortek lamp has twice the light absorbed in the back cell. Given the aforementioned intensity (28) dependence which characterizes the degradation, it would appear at first glance that serious errors might ensue from the use of these lamps to measure the degradation of multijunction devices.

We have attempted to model the degradation of a triple-junction cell under the various light sources. This was done by calculating the degradation of each component (single junction) cell and then evaluating the performance of a triple-stack cell made by (mathematically) connecting the three cells in series. The rates of degradation for the single junction (component) cells under an AM1.5 light source were assumed to be as given in **Figure 4-3**. For a "balanced" triple-junction cell in which the same current is generated in each junction, the number of photons absorbed in each component cell is approximately 1/3 the number which would be absorbed if the component cell were measured as a single junction cell. Using **Equation 3**, we can predict that a cell illuminated at 1/3 AM1.5 will degrade the same amount in 1000 hours as will an equivalent "stand-alone" single junction cell which is degraded for 138 hours at AM1.5, i.e.:

$$(1 * AM1.5)^{1.8} * 138 \text{Hours} = (0.3333 * AM1.5)^{1.8} * 1000 \text{Hours} \qquad (3)$$
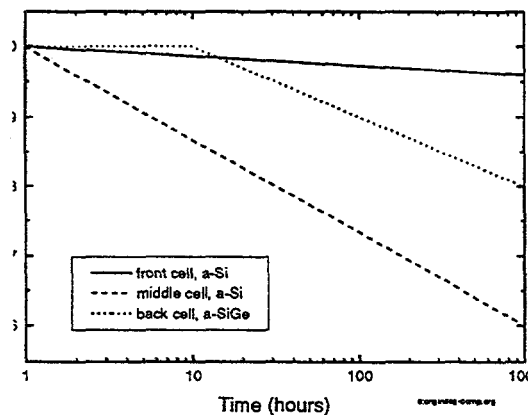
Figure 4-3. Idealized degradation curves used for modeling of triple-junction cells.

Thus, for a triple-junction cell light-soaked at AM1.5, the amount of degradation which should occur in each component can be determined from the three degradation curves in **Figure 4-3**. Using this analysis, we calculate that a triple-junction cell should degrade approximately 18.7% at AM1.5. For the other light sources, the nominal light intensity for each component cell, 0.333 AM1.5, must be modified by the ratio given in **Table 4-2**. For the middle cell of a triple, degraded for 1000 hours on a Na vapor lamp, the appropriate length of time to use in calculating the performance of this component in **Figure 4-3** is $(0.3333*1.89)^{1.8} * 1000$ hours = 435 hours.

Tables 4-3 and **4-4** give the initial, undegraded parameters for the components of a hypothetical triple-junction cell, and for the composite triple-junction cell. The procedure described above was used to calculate the degradation of each component of the triple-under the different light sources. The results of these calculations are presented in **Table 4-5**. As expected, the error induced by degrading the front cell with the incorrect light intensity is of no consequence. However, it is only the logarithmic dependence of performance on light-soak time (see **Figure 4-3**) which serves to reduce the impact of the relatively large deviations of the intensity of the Na vapor lamp and the Vortek lamp from the AM1.5 spectrum.

36

Table 4-3. Undegraded Cell Parameters.

J (rev. bias) [mA/cm^2]	V$_{oc}$ [V]	FF	component	J$_{sc}$ [mA/cm^2]	Efficiency [%]
6.6	0.82	0.71	front cell	6.385	3.717
6.6	0.82	0.71	middle cell	6.385	3.717
6.6	0.6	0.61	back cell	6.132	2.244

Table 4-4. Initial Triple-Junction Performance.

2.24	V$_{oc}$, Volts
6.32	J$_{sc}$, mA/cm^2
0.676	FF
9.57	Efficiency

Table 4-5. Normalized Efficiency of Components and Composite Triple-Junction Cell After 1000 Hours Light-soaking Under Various Light Sources.

	AM1.5	Na vapor lamp	Vortek arc lamp
front	0.943	0.947	0.954
middle	0.715	0.642	0.768
back	0.816	0.791	0.717
triple-junction	0.813	0.774	0.794

Another problem occurs with efforts to degrade multijunction cells at the maximum power point. For both the Vortek and Na vapor lamps, a cell which is current-balanced at AM1.5 will be front-limited when light-soaked on these lamps (see **Table 4-2**) due to the low illumination levels at short wavelength. Attempting to degrade such a cell at the maximum power point will push the load point of the front cell toward J$_{sc}$, imperceptibly improving the stability of the most stable component of the triple-junction device, while pushing the load points of the other cells toward V$_{oc}$ and thereby reducing the stability of those junctions. **Based on these considerations, light-soaking at the max. power point is probably only worthwhile outdoors.**

One last word of caution is in order regarding the degradation of multijunction cells on non-ideal light sources. The errors incurred when degrading multijunction cells of various designs will not be the same. For example, the error in degrading a triple-junction cell on the Vortek arc lamp is not particularly severe, as the over-illumination of the back cell is partially compensated by the under-illumination of the middle cell. However, a "thin" tandem cell (particularly an a-Si:H/a-Si:H tandem), having a QE similar to that shown in **Figure 4-4** will be grossly under-illuminated on the Vortek lamp. Hence, caution should be exercised in using this data quantitatively.
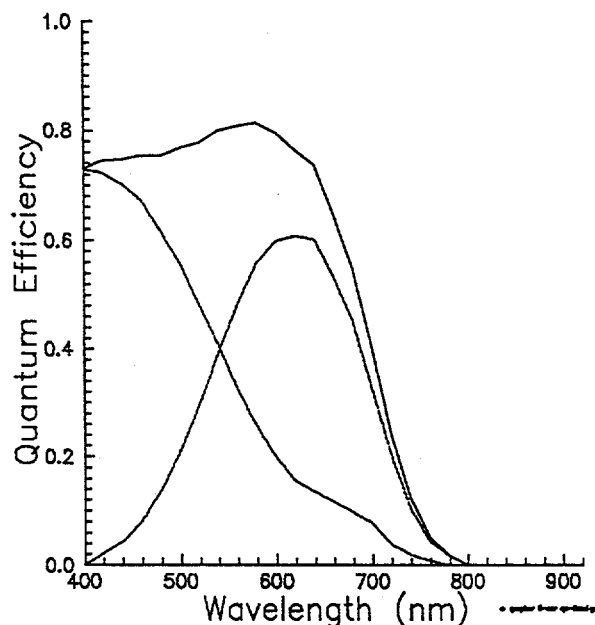
Figure 4-4. QE of a "standard" a-Si:H/a-Si:H tandem device.

4.2   Initial Module Performance - Influence of Simulators

The measurement of triple-junction cells and modules is complicated by the sensitivity of their performance to the insolation spectra and the measuring instrument. We have previously noted that the Spire simulator present at NREL and Solarex need considerable modification before they can be used for reliable measurements.

Table 4-6 illustrates the difference obtained for measurements of a large number of triple-junction modules measured on two Spire simulators, Spire #1 (Model 240D) and Spire #2 (Model 240A), and outdoors. Differences in the measurements of as much as 8% are found. Because of the extensive calibration and reliability of measurements on Spire #1, we consider measurements on that instrument to be most accurate.

38

Table 4-6. Modules Measured Under Different Conditions at Solarex.

Mod. #	Spire 2	Spire 1	Spire 2	Spire 1	Out-door 3/9/92	Out-door 3/12/92	Out/ Spire 1 (3/12)	
M2037.1								
V_{oc}	60.22	59.92	1.005	0%	58.4	60.5	1.01	i1: 800A, 1.74 eV
I_{sc}	197.1	205	0.961	-4%	193.1	190.5	0.929	i2: 4000A, 1.74 eV
FF	0.679	0.686	0.99	-1%	0.673	0.681	0.993	i3: 1600A, 1.45 eV
Eff, Aper.	10.21	10.68	0.956	-4%	9.62	9.95	0.932	
				Intensity:	101.5	100.8		
M2043.1								
V_{oc}	58.91	58.67	1.004	0%	54.7	60.1	1.024	i1: 720A, 1.74 eV
I_{sc}	199	200	0.995	-1%	198.8	192.8	0.964	i2: 4000A, 1.74 eV
FF	0.683	0.706	0.967	-3%	0.693	0.682	0.966	i3: 1600A, 1.43 eV
Eff, Aper.	10.14	10.5	0.966	-3%	9.55	10.02	0.954	
				Intensity:	114.2	102.2		
M2037.3								
V_{oc}	59.67	59.34	1.006	1%	57.9	59.7	1.006	i1: 800A, 1.74 eV
I_{sc}	194.6	211	0.922	-8%	193.9	189.8	0.900	i2: 4000A, 1.74 eV
FF	0.691	0.684	1.010	1%	0.69	0.686	1.003	i3: 1900A, 1.44 eV
Eff, Aper.	10.17	10.85	0.937	-6%	9.84	9.84	0.907	
				Intensity:	105.7	102.7		
M2055.3								
V_{oc}	59.72	59.57	1.003	0%	57.9	59.7	1.002	i1: 720A, 1.74 eV
I_{sc}	184.8	194	0.953	-5%	179.4	178.4	0.920	i2: 3000A, 1.74 eV
FF	0.694	0.707	0.982	-2%	0.706	0.709	1.003	i3: 1900A, 1.50 eV
Eff, Aper.	9.71	10.36	0.937	-6%	9.29	9.58	0.925	
				Intensity:	109.2	104.8		
D2045.1								
V_{oc}	60.4	60.1	1.005	0%	59.5	60.4	1.005	i1: 600A, 1.74 eV
I_{sc}	191.6	188	1.019	2%	187.6	188.9	1.005	i2: 4000A, 1.74 eV
FF	0.67	0.698	0.96	-4%	0.688	0.672	0.963	i3: 1600A, 1.48 eV
Eff, Aper.	9.82	9.99	0.983	-2%	9.73	9.72	0.973	
				Intensity:	103.9	102.7		
M2048.1								
V_{oc}	59.08	58.87	1.004	0%	58.3	58.9	1.001	i1: 720A, 1.74 eV
I_{sc}	192.8	206	0.936	-6%	187.7	185.3	0.900	i2: 4000A, 1.74 eV
FF	0.702	0.695	1.01	1%	0.706	0.711	1.023	i3: 1600A, 1.44 eV
Eff, Aper.	10.13	10.68	0.949	-5%	9.80	9.84	0.921	
				Intensity:	109.8	102.5		

Mod. #	Spire 2	Spire 1	Spire 2	Spire 1	Out-door 3/9/92	Out-door 3/12/92	Out/ Spire 1 (3/12)	
D2052.3								low Fe, triple-frit 3000A, i2
V_{oc}	59.22	58.85	1.006	1%	58.4	59.0	1.003	
I_{sc}	193.2	195	0.991	-1%	184.6	183.0	0.938	
FF	0.658	0.665	0.989	-1%	0.672	0.671	1.009	
Eff, Aper.	9.55	9.67	0.988	-1%	9.17	9.19	0.950	
				Intensity:	108.4	101.7		
M2030.3								low Fe, triple-frit 4000A, i2
V_{oc}	60.11	59.82	1.005	0%	58.2	60.2	1.006	
I_{sc}	198.9	205	0.97	-3%	196.8	193.5	0.944	
FF	0.675	0.687	0.983	-2%	0.681	0.685	0.997	
Eff, Aper.	10.23	10.67	0.959	-4%	9.88	10.11	0.948	
				Intensity:	109.2	99.7		
M2050.4								low Fe, triple-frit 4000A, i2
V_{oc}	58.12	57.73	1.007	1%	57.1	57.8	1.001	
I_{sc}	196.4	195	1.007	1%	193	193.2	0.991	
FF	0.656	0.682	0.962	-4%	0.656	0.662	0.971	
Eff, Aper.	9.49	9.74	0.974	-3%	9.17	9.36	0.961	
				Intensity:	105.2	99.9		

4.3 Impact of Shunts on Module Performance and Stability

By placing an isolation scribe an inch inside the edge of the substrate on two sides of the module and thereby excluding the regions of the module which contain the greatest amount of SnO_2 debris, the number of shunts on our modules has been effectively reduced. **Figure 4-5** shows a histogram of 33 modules which were recently made on a particular system. Of the four poorest modules in this group, one had an Al rear contact, and the other three had multiple segments which had high leakage currents. The tightness of the distribution (and the high value of its midpoint) indicates the extent to which the shunt problem has been reduced.

On the other hand, pinning down the impact of shunts on stability is not easily accomplished. **Table 4-7** shows data regarding the electrical curing of modules and gives light-soaking results. For seven of the eight modules, at least six segments "cured" after light-soaking. However, the shift in the distribution of leakage currents (measured at -2V, in the dark) toward higher values after light-soaking (and electrical curing) was not sufficient to have a dramatic impact on performance. The greatest increase in normalized efficiency for this group of modules after electrical curing was from 0.77 to 0.81. **Figure 4-6** illustrates this effect for another module. After 1000 hours of light-soaking the normalized efficiency (0.733) of this module was lower than expected. After electrically curing the module, the normalized efficiency improved to 0.78.
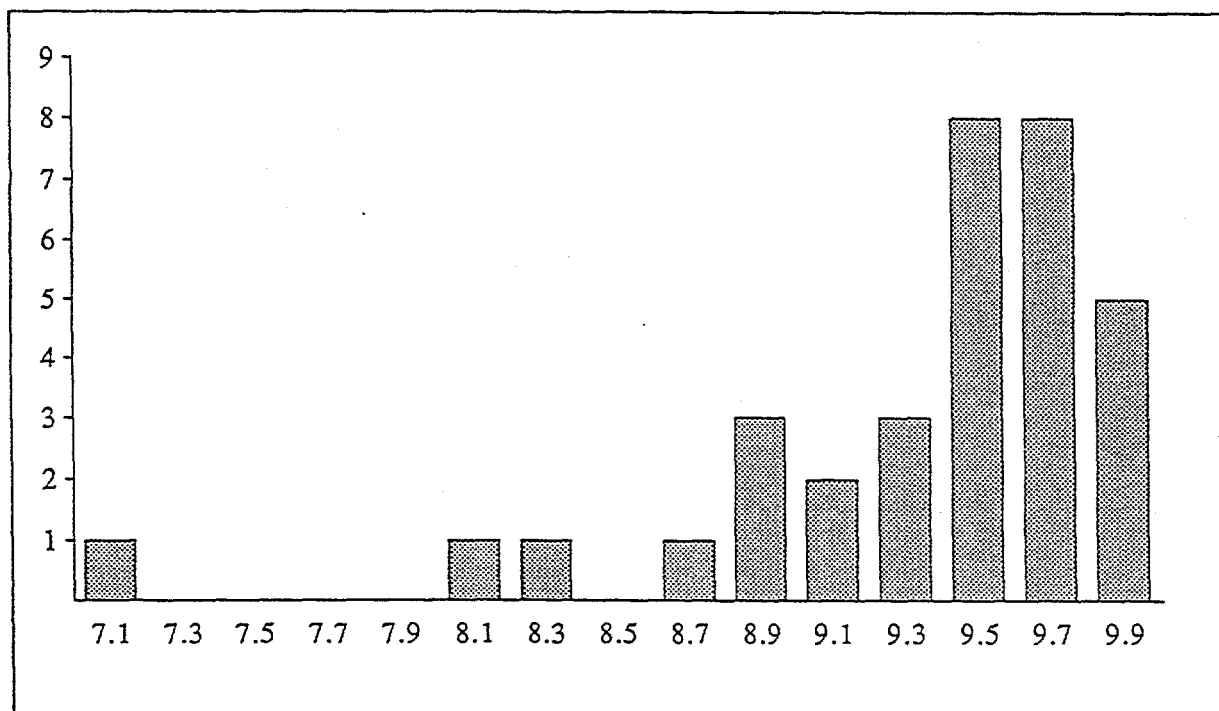
40

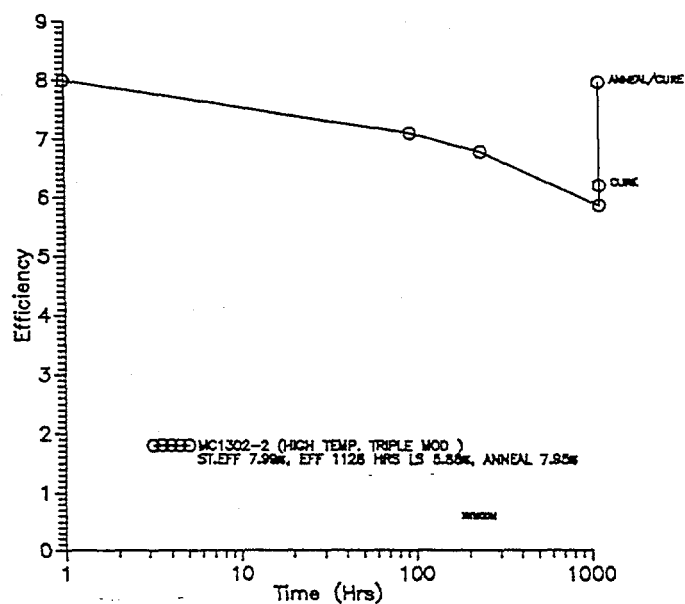**Figure 4-5.** Performance of recent modules made on the M system.

Figure 4-6. Module exhibiting partial recovery upon electrical cure.

Table 4-7. Increase in Leakage Current for Light-soaked Modules.

	# Segs. <1 mA	#1 to 10 mA	#11 to 25 mA	#26 to 100 mA	#> 100 mA	# which cured after light-soak	hrs light-soaked	init. eff.	light-soaked eff. (before cure)	norm. light-soaked eff.	eff. after cure	norm. eff. after cure
C1253.2	3	23					861	8.61	6.88	0.8	7.03	0.81
	0	25	1			6						
M1266.1		22	4				861	8.7	6.7	0.77	7.02	0.81
		14	10	2		13						
M1224.1		18	4	1+ (1)	0+ (2)			9.05			8.43	0.93
		7	5	8		17						
M1262.3	4	22					930	8.48	6.58	0.78	6.76	0.8
		22	4			13						
A1298.2		26					340	9.01	7.47	0.83	7.56	0.84
	7	18	1			6						
M1267.2	4	21	1				204	8.82	6.99	0.79	6.83	0.77
		21	3		2	6						
M2035.3		21	3	2			282	9.66	7.42	0.77	7.33	0.76
	3	13	4	6		9						
C2028.2	15	11					567	8.52	5.98	0.7	5.98	0.7
	n. m.											

Three "bad" segments were shorted out on M1224-1 before light-soaking.

cure data: For each module, the numbers in first row are the number of segments in the given range after the original cure, but before light-soaking. The numbers in the second row are the number of segments which were in the indicated range after curing the segments subsequent to light-soaking.

In an experiment on small area cells, laser pinholes were made in the a-Si:H before metallization. **Table 4-8** summarizes the leakage current measurements for 13 cells on one 3 in. x 3 in. substrate. Seven cells had laser pinholes and six did not. After electrical cure the leakage current for the laser-pinhole cells was greatly reduced, although none of these cells was judged to have an low leakage current. It was also noted that all seven of the laser pinhole cells exhibited a "flicker" behavior or "unstable" characteristic in the reverse bias leakage current. These

Table 4-8. Laser Pinhole Experiment - M1228-1-12, 7000Å Single Junction Control Cells. Leakage Currents Measured in the Dark on a Curve-Tracer.

Cell #	Before Cure, -.1V	After Cure, -.1V	After Cure, -2V	Note:
Cells Having Pinholes				
S1	5 mA	16 μA	0.6 mA	flicker
S3	5 mA	1 μA	18 μA	flicker, unstable
S4	6 mA	1 μA	0.4 mA	unstable
S5	6 mA	4.8 μA	0.18 mA	flicker
S7	6 mA	2 μA	5 mA	flicker, unstable
S8	5 mA	0.3 μA	150 mA	flicker, unstable
M1	4 mA	0.2 μA	0.6 mA	flicker, unstable
Cells Without Pinholes				
S2	0.2 μA	0.3 μA	6 μA	
S6	1.4 mA	7 μA	0.18 mA	
S9	0.2 μA	0.3 μA	1 μA	
M2	0.8 μA	1 μA	3 μA	
M3	2 μA	3 μA	40 μA	
M4	0.8 μA	1 μA	3 μA	

characteristics are often seen when large area segments on modules are electrically cured. Since none of the cells without laser pinholes showed these characteristics, it appears that the act of electrically curing a shunt may not be completely benign. When these cells were light-soaked (see **Figure 4-7**), the behavior of the laser pinhole cells was more erratic, with the degraded efficiencies spread over a wider range, and with some evidence of re-curing effects having occurred. These results provide additional evidence for explaining the difficulty which occurs in trying to pin down the effect of shunts on stability.
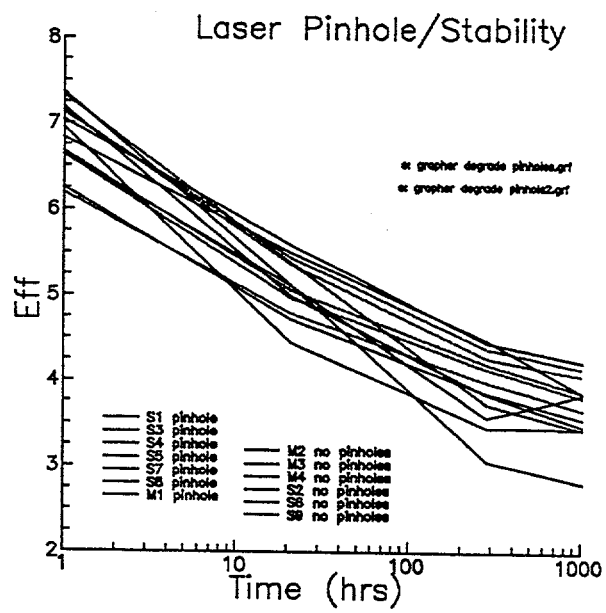
Figure 4-7. Differences in degradation of small area cells depending on the presence of pinholes.

44

REFERENCES

1. A. Matsuda and K. Tanaka, J. Non-Cryst. Solids 97 & 98, 1367 (1987); J. Appl. Phys. **60**, 4025.

2. Y.-M. Li and B.F. Fieselmann, Appl. Phys. Lett. **59**, 1720 (1991).

3. A. Catalano, R.R. Arya, M. Bennett, L. Chen, R. D'Aiello, B. Fieselmann, Y. Li, J. Newton, R. Podlesny, S. Wiedeman and L. Yang, "Research on Stable, High Efficiency Amorphous Silicon Multijunction Modules", Phase II Semi-Annual Technical Progress Report for the Period 1 May 1991 to 31 October 1991, NREL Contract No. ZM-0-19033-1.

4. Y.-M. Li, B.F. Fieselmann and A. Catalano, Proceedings of the 22nd IEEE Photovoltaic Specialists Conference (IEEE, N.Y., 1991), p. 1231.

5. See, for instance, A. Catalano in p. 9 of *Amorphous and Microcrystalline Semiconductor Devices: Optoelectronic Devices*, edited by J. Kanicki, Artech House, Boston (1991).

6. L. Yang, L. Chen and A. Catalano, Appl. Phys. Lett. **59**, 840 (1991).

7. Y. Ichikawa, S. Fujikake, H. Ohta, T. Sasaki and H. Sakai, Proceedings of the 22nd IEEE Photovoltaic Specialists Conference (IEEE, N.Y., 1991), p. 1296.

8. G. Ganguly, C. De, S. Ray, and A.K. Barua, J. Appl. Phys. **67** (1991), p. 3915.

9. M. Stutzmann, W. Jackson, and C. Tsai, Phys. Rev. B32, **23** (1985).

10. D. Redfield and R.H. Bube, Appl. Phys. Lett. **54**, 1037 (1989).

11. See e.g., the review by H.M. Branz, R.S. Crandall, and M. Silver, in AIP Conf. Proc. **234**, 29, (1991).

12. D. Redfield and R. Bube, Phys. Rev. Lett. **65**, 464 (1990).

13. L. Yang, L. Chen and A. Catalano, Appl. Phys. Lett. **59**, 842 (1991).

14. L. Yang and L. Chen, unpublished.

15. X. Li and S. Wagner, Mat. Res. Soc. Symp. Proc. (MRS, Pittsburgh, 1992) to be published.

16. S. Wagner, X. Xu, X.R. Li, D.S. Shen, M. Isomura, M. Bennett, A.E. Delahoy, X. Li, J.K. Arch, J.L. Nicque and S.J. Fonash, Proceedings of the 22nd IEEE Photovoltaic Specialists Conference (IEEE, N.Y., 1991), p. 1307.

17. M.S. Bennett, J.L. Newton, and K. Rajan, AIP Conf. Proc. **157**, 544 (1987).

18. Y. Nakata, H. Sannomiya, S. Moriuchi, A. Yokota, Y. Inoue, M. Itoh, and H. Itoh, Mat. Res. Soc. Symp. Proc., Vol. 192 (MRS, Pittsburgh, 1990), p. 25.

19. R.A. Street, AIP Conf. Proc. **234**, 21 (1991).

20. M. Stutzmann, in *Festkörperprobleme* (Advances in Solid State Physics), edited by U. Rössler (Vieweg, Braunschweig, 1988), Vol. **25**, p. 1.

21. P.J. McElheny, P. Chatterjie, and S.J. Fonash, J. Appl. Phys. **69**, 7674 (1991).

22. L. Yang, B. Abeles, W. Eberhardt and H. Stasiewski, Phys. Rev. 39, 3801 (1989).

23. W. Kruhler, H. Pfleiderer, R. Plattner, and W. Stetter, AIP Conf. Proc. **120**, 311 (1984).

24. C. Kittel, <u>Introduction to Solid State Physics</u>, Wiley, 5th ed., 1976, p. 210.

25. C.K. Lau, S.K. Tiku, and K.M. Lakin, J. Electrochem. Soc., 127, 1843 (1980).

26. S. Oda, H. Tokunaga, H. Kitajima, J. Hanna, I. Simizu and H. Kodado, Jpn. J. Appl. Phys., 24, 1606 (1985).

27. R. Gordon, J. Hu, J. Musher, and C. Giunta, Final Technical Report, NREL Subcontract # XG-0-19121-1, February, 1991.

28. H.C. Weller, R.H. Mauch, G.H. Bauer, Proceedings of the 22nd IEEE Photovoltaic Specialists Conference (IEEE, N.Y., 1991), pp. 1290-1295.

Document Control Page	1. NREL Report No. NREL/TP-411-4995	2. NTIS Accession No. DE92010599	3. Recipient's Accession No.

4. Title and Subtitle

Research on Stable, High-Efficiency, Amorphous Silicon Multijunction Modules

5. Publication Date
August 1992

6.

7. Author(s)

A. Catalano, M. Bennett, L. Chen, R. D'Aiello, B. Fieselmann, Y. Li, J. Newton, R. Podlesny, L. Yang

8. Performing Organization Rept. No.

9. Performing Organization Name and Address

Solarex Thin Film Division
826 Newtown-Yardley Road
Newtown, PA 18940

10. Project/Task/Work Unit No.

PV241101

11. Contract (C) or Grant (G) No.

(C) ZM-0-19033-1

(G)

12. Sponsoring Organization Name and Address
National Renewable Energy Laboratory
1617 Cole Blvd.
Golden, CO 80401-3393

13. Type of Report & Period Covered

Technical Report
1 May 1991 - 30 April 1992

14.

15. Supplementary Notes
NREL technical monitor: W. Luft

16. Abstract (Limit: 200 words)

This report describes work to demonstrate a multijunction module with a "stabilized" efficiency (600 h, 50°C, AM1.5) of 10.5%. Triple-junction devices and modules using a-Si:H alloys with carbon and germanium were developed to meet program goals. ZnO was used to provide a high optical transmission front contact. Proof of concept was obtained for several important advances deemed to be important for obtaining high (12.5%) stabilized efficiency. They were (1) stable, high-quality a-SiC:H devices and (2) high-transmission, textured ZnO. Although these developments were not scaled up and included in modules, triple-junction module efficiencies as high as 10.85% were demonstrated. NREL measured 9.62% and 9.00% indoors and outdoors, respectively. The modules are expected to lose no more than 20% of their initial performance.

17. Document Analysis
a. Descriptors

photovoltaics ; solar cells ; high efficiency ; amorphous silicon ; multijunction ; modules

b. Identifiers/Open-Ended Terms

c. UC Categories
271

18. Availability Statement
National Technical Information Service
U.S. Department of Commerce
5285 Port Royal Road
Springfield, VA 22161

19. No. of Pages

57

20. Price

A04

Form No. 0069E (6-30-87)